Zirconium−Butadiene Bonded over a Planar Set of Oxygens Derived from Calix[4]arene and Its Behavior as a Source of Zirconium(II)

Alessandro Caselli, Luca Giannini, Euro Solari, and Carlo Floriani*

Institut de Chimie Minérale et Analytique, BCH, Université de Lausanne, CH-1015 Lausanne, Switzerland

Nazzareno Re

Dipartimento di Chimica, Università di Perugia, I-06100 Perugia, Italy

Angiola Chiesi-Villa and Corrado Rizzoli

Dipartimento di Chimica, Università di Parma, I-43100 Parma, Italy

Received July 22, 1997[⊗]

This report deals with the first examples of butadienes bonded to a Zr−O matrix provided by a calix[4]arene skeleton and their reactivity. The reaction of [{*p*-Bu^t-calix[4]-(OMe)$_2$-(O)$_2$}ZrCl$_2$], **2**, with Mg(C$_4$H$_6$)(thf)$_2$ and Mg(Ph$_2$C$_4$H$_4$)(thf)$_3$ led to [{*p*-Bu^t-calix[4]-(OMe)$_2$(O)$_2$}-Zr(η^4-C$_4$H$_6$)], **3**, and [{*p*-Bu^t-calix[4]-(OMe)$_2$(O)$_2$}Zr(η^4-Ph$_2$C$_4$H$_4$)], **4**. The butadiene fragment exhibits a π^2,η^4 bonding mode, as shown by an X-ray analysis on both compounds. Extended Hückel calculations confirmed the energetically preferred *s-cis* conformation and the π^2,η^4 bonding mode *vs* the σ^2,π,η^4 one. The parent compound **3** of this series behaves, however, both as a source of zirconium(II) in displacement reactions or as a dialkyl derivative of zirconium(IV) in insertion reactions. In the former class of transformations, the reaction of **3** with Ph$_2$CO and PhCOCOPh led to the dioxo metallacycles [{*p*-Bu^t-calix[4]-(OMe)$_2$(O)$_2$}-Zr{−OC(Ph)$_2$−C(Ph)$_2$O−}], **5**, and [{*p*-Bu^t-calix[4]-(OMe)$_2$(O)$_2$}Zr{−OC(Ph)═C(Ph)O−})], **6**, respectively. Butadiene was also displaced by diphenylacetylene leading to [{*p*-Bu^t-calix-[4]-(OMe)$_2$(O)$_2$}Zr(η^2-Ph$_2$C$_2$)], **7**, and by a phenylnitrene source [PhN$_3$] forming the dinuclear phenylimido-bridged complex [{*p*-Bu^t-calix[4]-(OMe)$_2$(O)$_2$}$_2$Zr$_2$(μ-NPh)$_2$], **8**. Unlike at room temperature, Ph$_2$CO reacted with **3** at low temperature without displacing the butadiene, but leading, instead, to the stepwise insertion of the ketone to form [{*p*-Bu^t-calix[4]-(OMe)$_2$(O)$_2$}Zr{CH$_2$CH═CHCH$_2$C(Ph)$_2$O}], **10**, and [{*p*-Bu^t-calix[4]-(OMe)$_2$(O)$_2$}Zr{−OC(Ph)$_2$-CH$_2$CH═CHCH$_2$C(Ph)$_2$O−}], **11**. Using 2 mol of acetone, [{*p*-Bu^t-calix[4]-(OMe)$_2$(O)$_2$}Zr{−OC(Me)$_2$CH$_2$CH═CHCH$_2$C(Me)$_2$O−}], **12**, was obtained. MeCN and EtCN inserted in a single Zr−C bond (of a formal σ^2,π,η^4 structure) yielding [{*p*-Bu^t-calix[4]-(OMe)$_2$(O)$_2$}Zr{−CH$_2$CH═CHCH$_2$C(Me)═N−}], **13**, and [{*p*-Bu^t-calix[4]-(OMe)$_2$(O)$_2$}Zr{−CH$_2$CH═CHCH$_2$-C(Et)═N−}], **14**. Bu^{t}NC engaged **3** in a multistep insertion reaction leading to [{*p*-Bu^t-calix[4]-(OMe)$_2$(O)$_2$}Zr{−(Bu^t)NC(C$_4$H$_6$)C(C═NBu^t)N(Bu^t)−}], **15**, *via* a pathway which has been observed in the reaction of Bu^{t}NC with dialkylzirconium calix[4]arene derivatives. The σ^2 behavior of butadiene in **3** was further verified in the reaction with H$_2$O to give [{*p*-Bu^t-calix[4]-(OMe)$_2$(O)$_2$}$_2$Zr$_2$(μ-O)$_2$], **9**, and butenes.

Introduction

The zirconium−diene fragment became one of the most widely used organometallic synthons, this work origining from the earlier investigation by Erker and Nakamura on [Cp$_2$Zr(butadiene)].[1] How much the ancillary ligand determines the reactivity of such a functionality still remains to be explored. Very few investigations in this field have moved away from cyclopentadienyl-type ligands.[2] Our recent approach in organometallic chemistry made use of dianionic macrocyclic ligands, which, by their conformation, allow the metal to have two *cis* coordination sites. They are the dibenzotetramethyltetraaza[14]annulene (**A**),[3] [tmtaa] and the calix[4]arene-dimethoxy dianion (**B**), [*p*-Bu^t-calix[4]-(OMe)$_2$(O)$_2$],[4] which provide a set of N$_4$ and O$_4$ atoms, respectively. In the latter case, we took advantage of a preorganized set of oxygen donor atoms of calix[4]arene[5] in an almost planar arrangement. This

⊗ Abstract published in *Advance ACS Abstracts,* November 15, 1997.

(1) (a) Yasuda, H.; Tatsumi, K.; Nakamura, A. *Acc. Chem. Res.* **1985**, *18*, 120. (b) Erker, G.; Krüger, C.; Müller, G. *Adv. Organomet. Chem.* **1985**, *24*, 1 and references therein.

(2) Fryzuk, M. D.; Haddad, T. S.; Rettig, S. J. *Organometallics* **1989**, *8*, 1723. Diamond, G. M.; Green, M. L. H.; Walker, N. M.; Howard, J. A. K. *J. Chem. Soc., Dalton Trans.* **1992**, 2641.

(3) (a) Giannini, L.; Solari, E.; Floriani, C.; Chiesi-Villa, A.; Rizzoli, C. *Angew. Chem., Int. Ed. Engl.* **1994**, *33*, 2204. (b) Giannini, L.; Solari, E.; De Angelis, S.; Ward, T. R.; Floriani, C.; Chiesi-Villa, A.; Rizzoli, C. *J. Am. Chem. Soc.* **1995**, *117*, 5801. (c) Floriani, C.; Ciurli, S.; Chiesi-Villa, A.; Guastini, C. *Angew. Chem., Int. Ed. Engl.* **1987**, *26*, 70.

(4) Giannini, L.; Solari, E.; Zanotti-Gerosa, A.; Floriani, C.; Chiesi-Villa, A.; Rizzoli, C. *Angew. Chem., Int. Ed. Engl.* **1996**, *35*, 85.

(5) (a) Gutsche, C. D. *Calixarenes*; The Royal Society of Chemistry: Cambridge, U.K., 1989. (b) *Calixarenes, A Versatile Class of Macrocyclic Compounds*; Vicens, J., Böhmer, V., Eds.; Kluwer: Dordrecht, The Netherlands, 1991.

S0276-7333(97)00624-9 CCC: $14.00

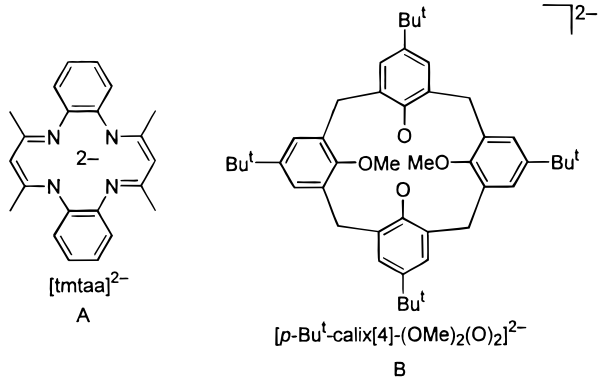

phenoxo matrix, in the case of zirconium, has been widely employed in exploring the chemistry of the Zr−C functionalities.[6] These studies, like the present one, have particular relevance with regard to a modeling approach to organometallic functionalities anchored to heterogeneous, oxygen-rich surfaces.[7]

We report here the related chemistry of the Zr−butadiene functionality supported by the calix[4]-dimethoxy dianion **B**. Unlike in the cyclopentadienyl series,[1b] butadiene displays, in the present case, exclusively the *s-cis* π^2,η^4 bonding mode to the metal, though its chemistry follows two general pathways. In the first one, butadiene behaves like a σ^2,π,η^4 system and, thus, functions in insertion reactions, while in the second pathway we observed displacement of the butadiene unit. Importantly, the [{*p*-Bu^t-calix[4]-$(OMe)_2(O)_2$}Zr-(η^4-C_4H_6)] functions as a source of zirconium(II). Preliminary results on the synthesis of the parent compound have been communicated.[4]

Experimental Section

General Procedure. All reactions were carried out under an atmosphere of purified nitrogen. Solvents were dried and distilled before use by standard methods. ^{1}H NMR and IR spectra were recorded on AC-200, DPX-400 Bruker, and Perkin-Elmer FT 1600 instruments. GC and GC-MS analyses were carried out using a HP 5890 Series II system and a HP 5890A GC system, respectively. The syntheses of [*p*-Bu^t-calix-[4]-$(OMe)_2(OH)_2$],[8] [*p*-Bu^t-calix[4]-$(OMe)_2(O)_2ZrCl_2$],[4] PhN_3,[9] $Mg(C_4H_6)(thf)_2$,[10] and $Mg(C_4H_6)(thf)_2$[11] have been performed as reported.

Synthesis of 3. **1** (29.2 g, 43.0 mmol) and $ZrCl_4(thf)_2$ (16.3 g, 43.0 mmol) were suspended in benzene (220 mL), and the reaction mixture refluxed for 2 h. The solvent was removed by distillation and then readded. After 10 min of refluxing, the solvent was removed by distillation and the residue dried *in vacuo* at 80 °C. The flask was then charged with fresh toluene (300 mL) and cooled to −40 °C, and to this mixture was added $[Mg(C_4H_6)(thf)_2]$ (10.1 g, 45.0 mmol). The reaction mixture was allowed to warm up to room temperature overnight, resulting in a dark red suspension. Volatiles were then removed *in vacuo*, and pentane (300 mL) was added to the residue. Extraction over 72 h gave **3** as an orange powder, which was then collected by filtration and finally dried *in vacuo* (30.4 g, 86%). Anal. Calcd for **3**, $C_{50}H_{64}O_4Zr$: C, 73.21; H, 7.86. Found: C, 73.30; H, 8.26. ^{1}H NMR (C_6D_6, 298 K): δ 7.27 (s, 4H, ArH), 6.80 (s, 4H, ArH), 5.97 (m, 2H, CH), 4.35 (br, 4H, *endo*-CH_2) overlapping with 4.35 (br, 6H, MeO), 3.49 (m, 2H, CH_2(3,4)), 3.21 (d, J = 12.5 Hz, 4H, *exo*-CH_2), 2.30 (m, 2H, CH_2(1,2)), 1.47 (s, 18H, Bu^t), 0.74 (s, 18H, Bu^t). ^{1}H NMR (C_7D_8, 298 K): δ 7.21 (s, 4H, ArH), 6.81 (s, 4H, ArH), 5.90 (m, 2H, CH), 4.32 (br, 4H, *endo*-CH_2) overlapping with 4.32 (br, 6H, MeO), 3.35 (m, 2H, CH_2(3,4)), 3.19 (d, 4H, *exo*-CH_2), 2.19 (m, 2H, CH_2(1,2)), 1.45 (s, 18H, Bu^t), 0.74 (s, 18H, Bu^t). ^{1}H NMR (C_7D_8, 245 K): δ 7.26 (s, 4H, ArH), 6.83 (s, 4H, ArH), 5.95 (m, 2H, CH), 4.54 (d, J = 12.4 Hz, 2H, *endo*-CH_2), 4.26 (s, 3H, MeO), 4.18 (d, J = 12.6 Hz, 2H, *endo*-CH_2), 3.62 (s, 3H, MeO), 3.46 (m, 2H, CH_2(3,4)), 3.23 (m, 4H, *exo*-CH_2), 2.27 (m, 2H, CH_2(1,2)), 1.51 (s, 18H, Bu^t), 0.71 (s, 18H, Bu^t). ^{1}H NMR (C_7D_8, 333 K): δ 7.17 (s, 4H, ArH), 6.77 (s, 4H, ArH), 5.85 (m, 2H, CH), 4.28 (d, J = 12.5 Hz, 4H, *endo*-CH_2), 4.13 (s, 6H, MeO), 3.26 (m, 2H, CH_2(3,4)), 3.14 (d, J = 12.5 Hz, 4H, *exo*-CH_2), 2.16 (m, 2H, CH_2(1,2)), 1.40 (s, 18H, Bu^t), 0.79 (s, 18H, Bu^t). Crystals suitable for X-ray analysis were obtained at room temperature by slow evaporation of a saturated solution of **3** in *n*-hexane.

Synthesis of 4. **2** (8.26 g, 8.66 mmol) and $Mg(C_{16}H_{14})(thf)_3$ (3.9 g, 8.7 mmol) were suspended in toluene (250 mL) at −30 °C. The mixture, which became deep red in seconds, was allowed to warm to room temperature while stirring. Dioxane (5 mL) was added, and the mixture was stirred for 1 h. Volatiles were then removed *in vacuo* (heating at 50 °C). The residue was extracted overnight with a mixture of hexane (230 mL) and benzene (30 mL). The red suspension was kept at −25 °C for 24 h to give **4** as a deep red microcrystalline solid, which was collected and dried *in vacuo* (5.79 g, 61.4%). Anal. Calcd for **4**·$(C_6H_6)_{1.5}$, $C_{71}H_{81}O_4Zr$: C, 78.26; H, 7.49. Found: C, 78.31; H, 7.73. ^{1}H NMR (C_6D_6, 298 K): δ 7.36−6.63 (m, 27H, ArH, benzene), 6.07 (m, 2H, H(5,6)), 4.48 (s, 3H, MeO), 4.31 (d, J = 12.5 Hz, 2H, *endo*-CH_2), 4.00 (m, 2H, H(1,2)), 3.92 (d, 2H, *endo*-CH_2) overlapping with 3.89 (s, 3H, MeO), 3.30 (d, J = 12.5 Hz, 2H, *exo*-CH_2), 2.94 (d, J = 12.5 Hz, 2H, *exo*-CH_2), 1.37 (s,18H, Bu^t), 0.70 (s, 9H, Bu^t), 0.64 (s, 9H, Bu^t). ^{1}H NMR (CD_2Cl_2, 298 K): δ 7.37−6.50 (m, 27H, ArH, benzene), 6.09 (m, 2H, H(5,6)), 4.97 (s, 3H, MeO), 4.72 (s, 3H, MeO), 4.29 (d, J = 12.5 Hz, 2H, *endo*-CH_2), 3.80 (m, 2H, H(1,2)) overlapping with 3.72 (d, 2H, *endo*-CH_2), 3.32 (d, J = 12.5 Hz, 2H, *exo*-CH_2), 2.86 (d, J = 12.5 Hz, 2H, *exo*-CH_2), 1.20 (s, 18H, Bu^t), 1.06 (s, 9H, Bu^t), 1.00 (s, 9H, Bu^t). Crystals suitable for X-ray analysis were obtained at room temperature from a supersaturated solution of **4** in hexane/benzene (10:1).

Synthesis of 5. A solution of Ph_2CO (1.13 g, 6.38 mmol) in toluene (50 mL) was added dropwise to a solution of **3** (2.73 g, 3.33 mmol) in toluene (50 mL), and the resulting clear yellow solution was stirred for 2 h. Volatiles were removed *in vacuo*, and *n*-hexane (30 mL) was added to the residue. White crystals of **5**·C_7H_8 were then collected and dried *in vacuo* (2.22 g, 55%). Anal. Calcd for **5**·C_7H_8, $C_{79}H_{86}O_6Zr$: C, 77.60; H, 7.09. Found: C, 77.49; H, 7.37. ^{1}H NMR (C_6D_6, 298 K): δ 7.96 (m, 8H, Ph), 7.26 (s, 4H, ArH), 7.13−6.98 (m, 17H, Ph, toluene), 6.84 (s, 4H, ArH), 4.50 (d, J = 12.4 Hz, 4H, *endo*-CH_2), 3.95 (s, 6H, MeO), 3.22 (d, J = 12.4 Hz, 4H, *exo*-CH_2), 2.10 (s, 3H, toluene), 1.45 (s, 18H, Bu^t), 0.80 (s, 18H, Bu^t).

Synthesis of 6. A solution of PhCOCOPh (0.71 g, 3.38 mmol) in toluene (50 mL) was added to a solution of **3** (2.73 g, 3.33 mmol) in toluene (50 mL), and the resulting green solution was stirred for 2 h. Volatiles were removed *in vacuo*, *n*-hexane (60 mL) was added to the residue, and the resulting solution was kept at −24 °C for 1 day. **6**·C_7H_8 precipitated as a green powder, which was then collected and dried *in vacuo* (2.56 g,

(6) (a) Giannini, L.; Caselli, A.; Solari, E.; Floriani, C.; Chiesi-Villa, A.; Rizzoli, C.; Re, N.; Sgamellotti, A. *J. Am. Chem. Soc.* **1997**, *119*, 9198. (b) Giannini, L.; Caselli, A.; Solari, E.; Floriani, C.; Chiesi-Villa, A.; Rizzoli, C.; Re, N.; Sgamellotti, A. *J. Am. Chem. Soc.* **1997**, *119*, 9709.

(7) (a) Corker, J.; Lefebvre, F.; Lecuyer, C.; Dufaud, V.; Quignard, F.; Choplin, A.; Evans, J.; Basset, J.-M. *Science* **1996**, *271*, 966. (b) Niccolai, G. P.; Basset, J.-M. *Appl. Catal., A* **1996**, *146*, 145. (c) Vidal, V.; Theolier, A.; Thivolle-Cazat, J.; Basset, J.-M.; Corker, J. *J. Am. Chem. Soc.* **1996**, *118*, 4595.

(8) Arduini, A.; Casnati, A. In *Macrocycle Synthesis*; Parker, O., Ed.; Oxford University Press: New York, 1996; Chapter 7.

(9) Lindsay, R. O.; Allen, C. F. H. *Organic Syntheses*; Wiley: New York, 1955; Collect. Vol. III, p 710.

(10) Fujita, K.; Ohnuma, Y.; Yasuda, H.; Tani, H. *J. Organomet. Chem.* **1976**, *113*, 201.

(11) Yasuda, H.; Kajihara, Y.; Mashima, K.; Nagasuna, K.; Lee, K.; Nakamura, A. *Organometallics* **1982**, *1*, 388.

65%). Anal. Calcd for **6**·C_7H_8, $C_{71}H_{82}O_6Zr$: C, 75.96; H, 7.36. Found: C, 75.29; H, 7.35. ^{1}H NMR (C_6D_6, 298 K): δ 8.06 (m, 4H, Ph), 7.26−7.00 (m, 15H, ArH, Ph, toluene), 6.79 (s, 4H, ArH), 4.40 (d, J = 12.5 Hz, 4H, *endo*-CH_2), 3.96 (s, 6H, MeO), 3.14 (d, J = 12.5 Hz, 4H, *exo*-CH_2), 2.10 (s, 3H, toluene), 1.46 (s, 18H, Bu^t), 0.72 (s, 18H, Bu^t).

Synthesis of 7. **3** (4.89 g, 5.96 mmol) and Ph_2C_2 (1.09 g, 6.11 mmol) were dissolved in toluene (175 mL). The reaction mixture was refluxed for 12 h, the resulting yellow solution was then filtered, and the volatiles were removed *in vacuo*. *n*-Hexane (60 mL) was added to the residue, and **7** was collected as a white solid (4.12 g, 73%). Anal. Calcd for **7**, $C_{60}H_{68}O_4Zr$: C, 76.31; H, 7.26. Found: C, 76.54; H, 7.28. ^{1}H NMR (C_6D_6, 298 K): δ 7.50 (m, 4H, ArH, Ph), 7.25 (s, 4H, ArH) overlapping with 7.24 (m, 4H, Ph), 6.98 (m, 2H, Ph), 6.83 (s, 4H, ArH), 4.50 (d, J = 12.4 Hz, 4H, *endo*-CH_2), 4.25 (s, 6H, MeO), 3.20 (d, J = 12.4 Hz, 4H, *exo*-CH_2), 1.45 (s, 18H, Bu^t), 0.80 (s, 18H, Bu^t). Crystals suitable for X-ray analysis were obtained at room temperature from a supersaturated toluene solution.

Synthesis of 8. A solution of PhN_3 (0.449 g, 3.77 mmol) in toluene (10 mL) was added dropwise to a stirred toluene (80 mL) solution of **3** (3.20 g, 3.77 mmol) cooled at −70 °C. The stirred reaction mixture was allowed to warm to room temperature overnight to give a light brown suspension. Volatiles were removed *in vacuo*, and *n*-hexane (40 mL) was added to the residue. **8** was collected as a white solid (1.60 g, 50%). Anal. Calcd for **8**, $C_{104}H_{126}N_2O_8Zr_2$: C, 72.85; H, 7.41; N, 1.63. Found: C, 72.42; H, 7.81; N, 1.26. ^{1}H NMR ($CDCl_3$, 298 K): δ 7.27 (m, 4H, Ph), 7.10 (m, 4H, ArH), 6.88 (m, 4H, ArH), 6.74 (m, 4H, ArH), 6.63 (m, 4H, ArH), 6.61 (m, 4H, Ph), 6.50 (m, 2H, Ph), 4.30 (s, 12H, OMe), 4.25 (d, J = 12.4 Hz, 4H, *endo*-CH_2), 3.35 (d, J = 12.4 Hz, 4H, *endo*-CH_2), 3.15 (d, J = 12.4 Hz, 4H, *exo*-CH_2), 2.57 (d, J = 12.4 Hz, 4H, *exo*-CH_2), 1.35 (s, 36H, Bu^t), 0.90 (s, 36H, Bu^t). Crystals suitable for X-ray analysis were obtained at room temperature from a supersaturated pentane solution.

Synthesis of 9. A solution of water (0.685 M in THF, 4.25 mmol) was added dropwise to a stirred THF (80 mL) solution of **3** (3.57 g, 4.35 mmol) cooled at −80 °C. The reaction mixture was allowed to warm to room temperature overnight. Volatiles were removed in *vacuo*, *n*-hexane (30 mL) was added to the residue, and **9**·thf·C_6H_{14} was collected as a white solid (1.53 g, 41%). Anal. Calcd for **9**·thf·C_6H_{14}, $C_{102}H_{138}O_{11}Zr_2$: C, 71.12; H, 8.07. Found: C, 71.09; H, 8.20. ^{1}H NMR (C_6D_6, 298 K): δ 7.26 (s, 8H, ArH), 6.91 (s, 8H, ArH), 4.61 (d, J = 12.4 Hz, 8H, *endo*-CH_2), 4.40 (s, 12H, MeO), 3.58 (m, 4H, thf), 3.26 (d, J = 12.4 Hz, 8H, *exo*-CH_2), 1.49 (s, 36H, Bu^t), 1.40 (m, 4H, thf), 1.23 (m, 8H, hex), 0.88 (s, 36H, Bu^t) overlapping with 0.88 (m, 6H, hex). Crystals suitable for X-ray analysis were obtained from a room-temperature saturated toluene/hexane solution.

Synthesis of 10. A solution of Ph_2CO (0.86 g, 4.74 mmol) in toluene (50 mL) was added dropwise to a cooled (−90 °C) stirred solution of **3** (3.88 g, 4.73 mmol) in toluene (150 mL). The resulting dark yellow solution was allowed to warm to room temperature overnight and then filtered, the volatiles were removed *in vacuo*, and finally *n*-hexane (50 mL) was added to the residue. White **10**·C_7H_8·$(C_6H_{14})_{0.5}$ was collected and dried *in vacuo* (2.9 g, 54%). Anal. Calcd for **10**·C_7H_8·$(C_6H_{14})_{0.5}$, $C_{87}H_{89}O_5Zr$: C, 77.07; H, 7.89. Found: C, 76.73; H, 8.10. ^{1}H NMR (C_6D_6, 298 K): δ 7.83 (m, 4H, Ph), 7.32 (s, 4H, ArH), 7.16−7.12 (m, 6H, Ph) overlapping with 7.14−6.98 (m, 5H, toluene), 6.85 (s, 4H, ArH), 6.56 (m, 1H, butadiene), 5.59 (m, 1H, butadiene), 4.63 (br, 4H, *endo*-CH_2), 3.62 (br, 6H, MeO) overlapping with 3.62 (br, 2H, butadiene), 3.28 (br, 4H, *exo*-CH_2), 3.08 (d, J = 10.7 Hz, 2H, butadiene), 2.10 (s, 3H, toluene), 1.49 (s, 18H, Bu^t), 1.23 (m, 4H, hexane), 0.88 (m, 3H, hexane), 0.76 (s, 18H, Bu^t). ^{1}H NMR (C_6D_6, 338 K): δ 7.81 (m, 4H, Ph), 7.30 (s, 4H, ArH), 7.15 (m, 6H, Ph) overlapping with 7.14−6.98 (m, 5H, toluene), 6.88 (s, 4H, ArH), 6.53 (m, 1H, butadiene), 5.56 (m, 1H, butadiene), 4.53 (d, J = 12.5 Hz, 4H, *endo*-CH_2), 3.60 (m, 2H, butadiene) overlapping with 3.59 (s, 6H, MeO), 3.28 (d, J = 12.5 Hz, 4H, *exo*-CH_2), 3.10 (d, J = 10.6 Hz, 2H, butadiene), 2.14 (s, 3H, toluene), 1.48 (s, 18H, Bu^t), 1.27 (m, 4H, hexane), 0.89 (m, 3H, hexane), 0.83 (s, 18H, Bu^t).

Synthesis of 11. A solution of Ph_2CO (0.57 g, 3.15 mmol) in toluene (40 mL) was added dropwise to a cooled (−90 °C) stirred solution of **3** (2.57 g, 3.14 mmol) in toluene (150 mL). The resulting dark yellow solution was allowed to warm to room temperature overnight. The ^{1}H NMR spectrum of the crude solution showed clean **10**. A solution of Ph_2CO (0.57 g, 3.15 mmol) in toluene (40 mL) was then added dropwise to the cooled (-90 °C), stirred reaction mixture. The resulting colorless solution was allowed to warm to room temperature and then filtered, the volatiles were removed *in vacuo*, and finally *n*-hexane (50 mL) was added to the residue. White **11**·$(C_6H_{14})_{0.5}$ was then collected and dried *in vacuo* (1.90 g, 49%). Anal. Calcd for **11**·$(C_6H_{14})_{0.5}$, $C_{79}H_{91}O_6Zr$: C, 77.28; H, 7.47. Found: C, 77.27; H, 7.90. ^{1}H NMR (C_7D_8, 298 K): δ 7.57−6.84 (m, 28H, ArH, Ph), 5.49 (m, 2H, butadiene), 4.63 (br, 4H, *endo*-CH_2), 4.00 (br, 6H, MeO), 3.69−2.93 (br, 4H, butadiene) overlapping with (br, 4H, *exo*-CH_2), 1.42 (s, 18H, Bu^t), 1.26 (m, 4H, hexane), 0.88 (m, 3H, hexane), 0.74 (s, 18H, Bu^t). ^{1}H NMR (C_7D_8, 372 K): δ 7.48 (m, 8H, Ph), 7.15 (s, 4H, ArH), 7.10−6.99 (m, 12H, Ph), 6.84 (s, 4H, ArH), 5.56 (m, 2H, butadiene), 4.17 (d, J = 12.8 Hz, 4H, *endo*-CH_2), 3.77 (s, 6H, MeO), 3.46 (m, 4H, butadiene), 3.12 (d, J = 12.8 Hz, 4H, *exo*-CH_2), 1.38 (s, 18H, Bu^t), 1.25 (m, 4H, hexane), 0.86 (m, 3H, hexane), 0.74 (s, 18H, Bu^t). ^{1}H NMR (C_7D_8, 263 K): δ 7.61 (m, 4H, Ph), 7.32 (m, 4H, Ph), 7.25 (s, 2H, ArH), 7.17−7.07 (m, 14H, ArH, Ph), 6.98 (s, 2H, ArH), 6.80 (s, 2H, ArH), 5.44 (m, 2H, butadiene), 4.67 (d, J = 12.8 Hz, 2H, *endo*-CH_2), 4.01 (s, 3H, MeO), 3.70 (m, 2H, butadiene), 3.56 (d, J = 12.8 Hz, 2H, *endo*-CH_2), 3.47 (d, J = 12.8 Hz, 2H, *exo*-CH_2), 3.39 (s, 3H, MeO), 3.09 (m, 2H, butadiene), 2.91 (d, J = 12.8 Hz, 2H, *exo*-CH_2), 1.42 (s, 18H, Bu^t), 1.26 (m, 4H, hexane), 0.88 (m, 3H, hexane), 0.77 (s, 9H, Bu^t), 0.71 (s, 9H, Bu^t).

Synthesis of 12. Acetone (1.00 mL, 13.6 mmol) was added to a stirred benzene (100 mL) solution of **3** (3.96 g, 4.83 mmol). The ^{1}H NMR (C_6D_6) spectrum of a dried sample showed that the reaction was complete, affording clean **12**. Volatiles were removed *in vacuo* from the colorless solution, and *n*-hexane (30 mL) was added to the residue. The flask was kept for 1 day at −24 °C, then the white **12**·$(C_6H_6)_{0.5}$ solid was collected and dried *in vacuo* (1.15 g, 24%). Anal. Calcd for **12**·$(C_6H_6)_{0.5}$, $C_{59}H_{79}O_6Zr$: C, 72.64; H, 8.16. Found: C, 72.65; H, 8.35. ^{1}H NMR (C_6D_6, 298 K): δ 7.36 (s, 4H, ArH), 6.96 (s, 4H, ArH), 5.32 (m, 2H, butadiene), 4.44 (d, J = 12.5 Hz, 4H, *endo*-CH_2), 3.87 (s, 6H, MeO), 3.44 (d, J = 12.5 Hz, 4H, *exo*-CH_2), 2.36 (m, 4H, butadiene), 1.49 (s, 18H, Bu^t), 1.24 (s, 12H, CH_3), 1.23 (m, 4H, hexane), 0.88 (m, 3H, hexane), 0.75 (s, 18H, Bu^t). Crystals suitable for X-ray analysis were obtained at room temperature from a saturated benzene solution.

Synthesis of 13. CH_3CN (0.156 g, 3.80 mmol) was added to a stirred solution of **3** (3.10 g, 3.77 mmol) in benzene(100 mL), yielding a yellow solution. The ^{1}H NMR (C_6D_6) spectrum showed that the reaction was complete, affording clean **13**. Volatiles were removed *in vacuo*, and *n*-hexane (30 mL) was added. The resulting suspension was stirred for 3 h, and **13**·C_6H_{14} was collected as a yellow solid and dried *in vacuo* (2.01 g, 56%). Anal. Calcd for **13**·C_6H_{14}, $C_{58}H_{81}NO_4Zr$: C, 73.52; H, 8.62; N, 1.48. Found: C, 73.30; H, 8.49; N, 1.34. ^{1}H NMR (C_6D_6, 298 K): δ 7.40−7.26 (m, 4H, ArH), 7.15 (m, 1H, butadiene) overlapping with C_6D_6, 6.96 (m, 2H, ArH), 6.87 (m, 2H, ArH), 6.56 (m, 1H, butadiene), 6.15 (m, 1H, butadiene), 5.51 (m, 1H, butadiene), 4.72 (d, J = 12.4 Hz, 1H, *endo*-CH_2), 4.64 (d, J = 12.0 Hz, 1H, *endo*-CH_2), 4.59 (d, J = 12.4 Hz, 1H, *endo*-CH_2), 4.51 (d, J = 12.4 Hz, 1H, *endo*-CH_2), 4.05 (s, 3H, MeO), 4.03 (s, 3H, OMe), 3.58 (m, 1H, butadiene), 3.40−3.31 (m, 4H, *exo*-CH_2), 2.11 (m, 1H, butadiene), 2.07 (s, 3H, CH_3), 1.59 (s, 9H, Bu^t), 1.57 (s, 9H, Bu^t), 1.23 (m, 8H, hexane), 0.88 (m, 6H, hexane), 0.86 (s, 9H, Bu^t), 0.83 (s, 9H, Bu^t).

Table 1. Experimental Data for the X-ray Diffraction Studies on Crystalline Complexes 3, 4, 7, 8, and 9

complex	**3**	**4**	**7**	**8**	**9**
formula	$C_{50}H_{64}O_4Zr$	$C_{62}H_{70}O_4Zr\cdot1.5C_6H_6$	$C_{60}H_{68}O_4Zr\cdot4.5C_7H_8$	$C_{104}H_{126}N_2O_8Zr_2\cdot4C_7H_8$	$C_{92}H_{116}O_{10}Zr_2\cdot C_7H_8\cdot2C_6H_{14}$
a, Å	10.411(2)	14.684(2)	28.846(5)	13.580(2)	12.375(2)
b, Å	12.931(3)	17.992(2)	17.387(3)	22.240(3)	40.636(5)
c, Å	34.344(7)	13.033(2)	30.241(5)	37.707(5)	21.083(3)
α, deg	90	109.64(1)	90	90	90
β, deg	98.72(2)	103.51(1)	90.19(3)	98.48(2)	103.91(2)
γ, deg	90	86.55(1)	90	90	90
V, Å^3	4570.1(17)	3152.6(8)	15167(5)	11264(3)	10291(3)
Z	4	2	8	4	4
fw	820.3	1087.6	1359.1	2083.2	1828.9
space group	$P2_1/c$	$P\bar{1}$	$C2/c$	$C2/c$	$C2/c$
T, °C	−130	20	−130	−130	−130
λ, Å	0.710 68	1.541 78	1.541 78	1.541 78	1.541 78
ρ_{calc}, g cm^{-3}	1.045	1.146	1.190	1.228	1.180
μ, cm^{-1}	2.74	17.71	15.64	19.64	20.91
transmission coeff	0.679−1.000	0.696−1.000	0.435−1.000	0.805−1.000	0.351−1.000
R1[a]	0.079	0.080	0.067	0.088	0.066
wR2[b]	0.215	0.249	0.197	0.248	0.198

[a] $R1 = \sum|\Delta F|/\sum|F_o|$ calculated on the unique observed data [$I > 2\sigma(I)$]. [b] $wR2 = [\sum w|\Delta F^2|^2/\sum w|F_o^2|^2]^{1/2}$ calculated on the unique total data with $I > 0$.

Synthesis of 14. CH_3CH_2CN (0.310 g, 5.64 mmol) was added to a stirred solution of **3** (4.63 g, 5.64 mmol) in toluene (125 mL) to give a yellow solution. The ^{1}H NMR (C_6D_6) spectrum showed that the reaction was complete, affording clean **14**. The toluene was concentrated to 25 mL, and *n*-hexane (75 mL) was added. The resulting solution was then filtrated and kept at −26 °C for 24 h. **14**·C_7H_8·$(C_6H_{14})_{0.5}$ was collected as a yellow solid and dried *in vacuo* (2.05 g, 37%). Anal. Calcd for **14**·C_7H_8·$(C_6H_{14})_{0.5}$, $C_{63}H_{84}NO_4Zr$: C, 74.88; H, 8.38; N, 1.39. Found: C, 74.57; H, 8.89; N, 1.21. ^{1}H NMR (C_6D_6, 298 K): *δ* 7.29−7.23 (m, 4H, ArH) overlapping with (m, 1H, butadiene), 7.14−6.95 (m, 5H, toluene), 6.85 (m, 2H, ArH), 6.76 (m, 2H, ArH), 6.46 (m, 1H, butadiene), 6.03 (m, 1H, butadiene), 5.43 (m, 1H, butadiene), 4.63−4.40 (m, 4H, *endo*-CH_2), 3.96 (s, 3H, MeO), 3.94 (s, 3H, OMe), 3.47 (m, 1H, butadiene), 3.28−3.21 (m, 4H, *exo*-CH_2), 2.20 (m, 2H, CH_2), 2.10 (s, 3H, toluene), 1.98 (m, 1H, butadiene), 1.48 (s, 9H, Bu^t), 1.46 (s, 9H, Bu^t), 1.23 (m, 4H, hexane), 1.18 (m, 3H, CH_3), 0.88 (m, 3H, hexane), 0.75 (s, 9H, Bu^t), 0.72 (s, 9H, Bu^t). Crystals suitable for X-ray analysis were obtained at −24 °C from a room-temperature saturated solution in benzene/pentane.

Synthesis of 15. A solution of Bu^{t}NC (1.13 g, 13.55 mmol) in toluene (49 mL) was added dropwise to a solution of **3** (3.71 g, 4.18 mmol) in toluene (100 mL). The resulting light orange solution was stirred for 2 h, volatiles were removed *in vacuo*, and *n*-hexane (50 mL) was added to the residue. **15**·$(C_6H_{14})_{0.5}$ was collected as a pale yellow powder (3.22 g, 64%). Anal. Calcd for **15**·$(C_6H_{14})_{0.5}$, $C_{69}H_{98}N_3O_4Zr$: C, 73.40; H, 8.88; N, 3.78. Found: C, 73.10; H, 8.95; N, 3.64. ^{1}H NMR (C_6D_6, 298 K): *δ* 7.39−7.32 (m, 4H, ArH), 6.99−6.89 (m, 4H, ArH), 5.74 (m, 2H, butadiene), 5.26 (d, J = 12.1 Hz, 1H, *endo*-CH_2), 5.05 (d, J = 12.0 Hz, 1H, *endo*-CH_2), 4,83 (d, J = 12.2 Hz, 1H, *endo*-CH_2), 4.70 (d, J = 12.1 Hz, 1H, *endo*-CH_2), 4.35 (s, 3H, MeO), 4.02 (s, 3H, MeO), 3.53 (m, 1H, butadiene), 3.47−3.27 (m, 4H, *exo*-CH_2), 2.85 (m, 1H, butadiene), 2.53 (m, 2H, butadiene), 1.60 (s, 9H, Bu^t), 1.53 (m, 9H, Bu^t), 1.48 (s, 9H, Bu^t), 1.43 (s, 9H, Bu^t), 1.25 (s, 9H, Bu^t) overlapping with 1.25 (m, 4H, hexane), 0.88 (m, 3H, hexane), 0.78 (s, 18H, Bu^t). IR (Nujol, ν_{max}/cm^{-1}): 1965.0 (s).

X-ray Crystallography for Complexes 3, 4, and 7−9. Suitable crystals were mounted in glass capillaries and sealed under nitrogen. The reduced cells were obtained with the use of TRACER.[12] Crystal data and details associated with data collection are given in Table 1 and in the Supporting Information (Table S1). Data were collected on a Rigaku AFC6S single-crystal diffractometer at 143 K for **3**, **7**, **8**, and **9** and 293 for **4**. For the intensities and background, the individual reflection profiles were analyzed.[13] The structure amplitudes were obtained after the usual Lorentz and polarization corrections, and the absolute scale was established by the Wilson method.[14] The crystal quality was tested by *ψ* scans showing that crystal absorption effects could not be neglected. The data were corrected for absorption using a semiempirical method.[15] The function minimized during the full-matrix least-square refinements was $\sum w(\Delta F^2)^2$. Weights were applied according to the scheme $w = 1/[\sigma^2(F_o^2) + (aP)^2]$ (with $P = (F_o^2 + 2F_c^2)/3$ and a = 0.1302, 0.1228, 0.1211, 0.2028, and 0.0989 for complexes **3**, **4**, **7**, **8**, and **9**, respectively. Anomalous scattering corrections were included in all structure factor calculations.[16b] Scattering factors for neutral atoms were taken from ref 16a for non-hydrogen atoms and from ref 17 for H atoms. Among the low-angle reflections, no correction for secondary extinction was deemed necessary.

All calculations were carried out on a Quansan personal computer equipped with an Intel Pentium processor. The structures were solved starting from three-dimensional Patterson maps using the observed reflections [$I > 2\sigma(I)$].[18] Structure refinements were based on the unique data having $I > 0$ using SHELX92.[19] Refinement was first done isotropically and then anisotropically for all non-H atoms, except for the disordered atoms.

In complex **3**, a ΔF map calculated after the isotropic refinement revealed a statistical distribution of the butadiene ligand over two positions (A and B). The two orientations, which do not share any atom, form a dihedral angle of 17.4-(82)°. Refinement of the relative occupancies resulted in a value of 0.65(2) and 0.35(2) for A and B, respectively.

In complex **4**, a statistical distribution around the C47···-C50 line in the diphenylbutadiene ligand was evident from a difference Fourier map calculated after the anisotropic refinement. The two orientations (A and B) of the butadiene framework share the C47, C50 terminal carbon atoms and form a dihedral angle of 21.0(14)° such that only C48 and C49 appear to be disordered. Refinement of the relative occupan-

(12) Lawton, S. L.; Jacobson, R. A. *TRACER (a cell reduction program)*; Ames Laboratory. Iowa State University of Science and Technology: Ames, IA, 1965.

(13) Lehmann, M .S.; Larsen, F. K. *Acta Crystallogr., Sect. A: Cryst. Phys., Diffr., Theor. Gen. Crystallogr.* **1974**, *A30*, 580−584.

(14) Wilson, A. J. C. *Nature* **1942**, *150*, 151.

(15) North, A. C. T.; Phillips, D. C.; Mathews, F. S. *Acta Crystallogr., Sect. A: Cryst. Phys., Diffr., Theor. Gen. Crystallogr.* **1968**, *A24*, 351.

(16) (a) *International Tables for X-ray Crystallography*; Kynoch Press: Birmingham, England, 1974; Vol. IV, p 99. (b) *Ibid*., p 149.

(17) Stewart, R. F.; Davidson, E. R.; Simpson, W. T. *J. Chem. Phys.* **1965**, *42*, 3175.

(18) Sheldrick, G. M. *SHELX76. Program for crystal structure determination*; University of Cambridge: Cambridge, England, 1976.

(19) Sheldrick, G. M. *SHELXL92. Program for Crystal Structure Refinement*; University of Göttingen: Göttingen, Germany, 1992.

Scheme 1

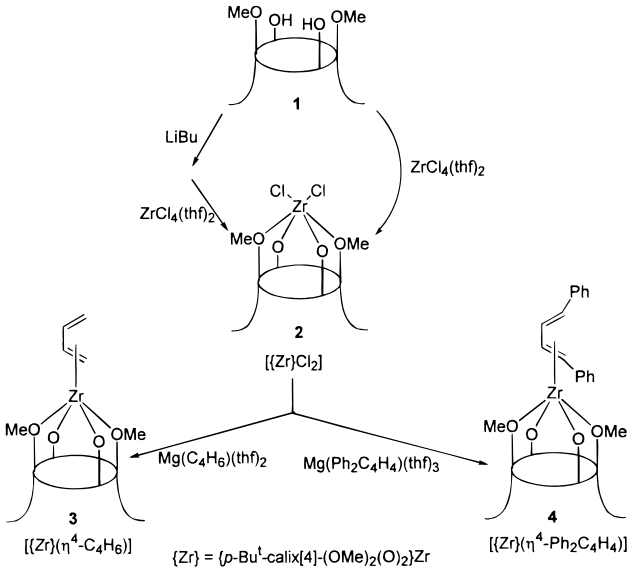

cies resulted in a value of 0.69(2) for C48A, C49A and 0.31(2) for C48B, C49B.

In addition, the toluene molecules in complexes **7**−**9**, some *tert*-butyl groups in complexes **3**, **4**, **8**, and **9**, and the *n*-hexane molecule in complex **9** were found to be affected by disorder. This was solved by considering the carbon atoms with higher thermal parameters as statistically distributed over two positions (A and B) and isotropically refined with the site occupation factors given in the Supporting Information (Table S2−S6). During the refinement, the aromatic rings of the disordered toluene molecules in complexes **7** and **8** were constrained to have a D_{6h} symmetry.

The hydrogen atoms, except those related to disordered carbon atoms, which were ignored, were put in geometrically calculated positions for **3** and **7**−**9** and located from a difference map for **4**. They were introduced in the subsequent refinement as fixed atom contribution with *U*'s fixed at 0.5 Å^2 for for **3** and **7**−**9** and at 0.12 Å^2 for **4**.

The final difference maps showed no unusual features, with no significant peaks above the general background except for a residual peak of 2.71 e Å^{-3} in **8** located midway along the Zr−N1 bond.

Final atomic coordinates are listed in the Supporting Information (Tables S2−S6 for non-H atoms and in Tables S7−S11 for hydrogens). Thermal parameters are also given in the Supporting Information (Tables S12−S16) in addition to bond distances and angles (Tables S17−S21).[20] Ordering information is given on any current masthead page.

Results and Discussion

Zr−Butadiene Derivatives. The synthesis of the parent compound used in this study, **3**, is displayed, along with the analogous diphenyl derivative, in Scheme 1. The reaction can be carried out either *via* the preliminary isolation of **2** or it can be performed *in situ* with the corresponding Mg−butadiene derivative. All the analytical and spectroscopic data are in agreement with the formulations reported for complexes **3** and **4**.

In solution, complex **4** has C_s symmetry; the ^{1}H NMR spectrum consists of two pairs of doublets for the bridging methylenes and two singlets for the methoxy groups. Below −10 °C (in toluene-d_8), complex **3** also exhibits a ^{1}H NMR spectrum characteristic of C_s symmetry. However, at temperatures above 40 °C, the spectrum simplifies and resembles that of a compound with C_{2v} symmetry (one pair of doublets for the bridging methylenes and a singlet for the methoxy groups). It is important to note that the splitting patterns for the butadiene protons of **3** are temperature independent (though the chemical shifts depend slightly on the temperature). The fact that the signals for the (3,4) and (1,2) protons in the butadiene ligand never coalesce proves that the dynamic process responsible for the increase in the apparent symmetry of complex **3** at high temperatures is not the flipping[21] of the butadiene fragment (involving a metallacyclopentene transition state). This observation is most likely due to the rotation[2] of butadiene.

Scheme 2

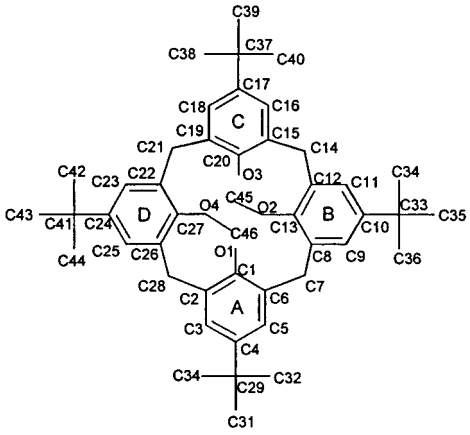

In the solid state, as shown by the X-ray analysis performed on single crystals of **3** and **4**, the bonding mode of the butadiene ligands in both complexes can be described as π^2,η^4. A variety of bonding modes of butadiene to zirconium ranging from π,η^4 to σ^2,π,η^4 can be found in complexes having subunits other than Cp_2-Zr.[2,3a,22] The structural and spectroscopic characteristics of the Zr−diene fragment in **3** and **4** are more closely related to the [(tmtaa)Zr][3a] derivatives (tmtaa = dibenzotetramethyltetraaza[14]annulene dianion) than the corresponding [Cp_2Zr][1,11,23,24] species. In particular, we can say that the *s-cis* form is the only butadiene conformer detected in the solid state; heating of **3** or **4** did not result in any *cis*−*trans* isomerization.[24,25]

The labeling scheme adopted for calixarene is given in Scheme 2. Selected bond distances and angles are quoted in Tables 2, 3, 4, 5, and 6 for complexes **3**, **4**, **7**,

(20) See paragraph at the end regarding Supporting Information.

(21) Erker, G.; Engel, K.; Krüger, C.; Chiang, A.-P. *Chem. Ber.* **1982**, *115*, 3311.

(22) Blenkers, J.; Hessen, B.; van Bolhuis, F.; Wagner, A. J.; Teuben, J. H. *Organometallics* **1987**, *6*, 459. Yasuda, H.; Nakamura, A. *Angew. Chem., Int. Ed. Engl.* **1987**, *26*, 723.

(23) Erker, G.; Dorf, U.; Benn, R.; Reinhardt, R.-D. *J. Am. Chem. Soc.* **1984**, *106*, 7649. Erker, G.; Lecht, R.; Petersen, J. L.; Bönnemann, H. *Organometallics* **1987**, *6*, 1962. Akita, M.; Matsuoka, K.; Asami, K.; Yasuda, H.; Nakamura, A. *J. Organomet. Chem.* **1987**, *327*, 193. Bürgi, H. B.; Dubler-Steude, K. C. *J. Am. Chem. Soc.* **1988**, *110*, 4953. Erker, G.; Aul, R. *Organometallics* **1988**, *7*, 2070. Erker, G.; Sosna, F.; Zwettler, R.; Krüger, C. *Organometallics* **1989**, *8*, 450. Yasuda, H.; Okamoto, T.; Matsuoka, Y.; Nakamura, A.; Kai, Y.; Kanehisa, N.; Kasai, N. *Organometallics* **1989**, *8*, 1139. Erker, G.; Friedrich, S.; Ralf, N. *Chem. Ber.* **1990**, *123*, 821. Erker, G.; Babil, M. *Chem. Ber.* **1990**, *123*, 1327. Beckhaus, R.; Wilbrandt, D.; Flatau, S.; Böhmer, H. *J. Organomet. Chem.* **1992**, *423*, 211.

(24) Erker, G.; Engel, K.; Korek, U.; Czisch, P.; Berke, H.; Caubère, P.; Vanderesse, R. *Organometallics* **1985**, *4*, 1531.

(25) Erker, G.; Wicker, J.; Engel, K.; Krüger, C. *Chem. Ber.* **1982**, *115*, 3300.

Table 2. Selected Bond Distances (Å) and Angles (deg) for Complex 3

Zr1−O1	1.990(6)	O1−C1	1.331(9)
Zr1−O2	2.349(6)	O2−C13	1.408(10)
Zr1−O3	1.988(6)	O2−C45	1.464(11)
Zr1−O4	2.360(5)	O3−C20	1.334(11)
Zr1−C47A	2.394(18)	O4−C27	1.407(12)
Zr1−C48A	2.398(17)	O4−C46	1.464(12)
Zr1−C49A	2.44(2)	C47A−C48A	1.44(2)
Zr1−C50A	2.525(16)	C48A−C49A	1.44(2)
Zr1−C47B	2.51(3)	C49A−C50A	1.41(2)
Zr1−C48B	2.39(3)	C47B−C48B	1.46(4)
Zr1−C49B	2.38(3)	C48B−C49B	1.45(4)
Zr1−C50B	2.38(4)	C49B−C50B	1.41(4)
C49B−Zr1−C50B	34.5(11)	Zr1−O2−C45	130.5(6)
C48B−Zr1−C49B	35.5(10)	Zr1−O2−C13	115.6(4)
C47B−Zr1−C48B	34.5(10)	C13−O2−C45	113.9(7)
C49A−Zr1−C50A	32.9(6)	Zr1−O3−C20	172.8(6)
C48A−Zr1−C49A	34.7(6)	Zr1−O4−C46	132.1(5)
C47A−Zr1−C48A	35.1(6)	Zr1−O4−C27	115.5(4)
O3−Zr1−O4	82.4(2)	C27−O4−C46	112.4(6)
O2−Zr1−O3	83.1(2)	C47A−C48A−C49A	114.9(15)
O1−Zr1−O4	82.4(2)	C48A−C49A−C50A	120.7(15)
O1−Zr1−O2	83.4(2)	C47B−C48B−C49B	114(2)
Zr1−O1−C1	171.3(5)	C48B−C49B−C50B	120(2)

Table 3. Selected Bond Distances (Å) and Angles (deg) for Complex 4

Zr1−O1	1.945(5)	O2−C45	1.434(16)
Zr1−O2	2.309(8)	O3−C20	1.348(10)
Zr1−O3	1.946(5)	O4−C27	1.433(12)
Zr1−O4	2.348(8)	O4−C46	1.463(15)
Zr1−C47	2.427(10)	C47−C48A	1.25(2)
Zr1−C48A	2.450(16)	C47−C48B	1.17(4)
Zr1−C49A	2.485(13)	C47−C57	1.477(15)
Zr1−C48B	2.58(3)	C48A−C49A	1.437(18)
Zr1−C49B	2.60(4)	C49A−C50	1.36(2)
Zr1−C50	2.505(12)	C48B−C49B	1.38(4)
O1−C1	1.353(10)	C49B−C50	1.18(4)
O2−C13	1.410(11)	C50−C51	1.498(14)
C49B−Zr1−C50	26.7(8)	C13−O2−C45	114.0(8)
C48B−Zr1−C49B	30.8(10)	Zr1−O3−C20	171.4(6)
C49A−Zr1−C50	31.6(4)	Zr1−O4−C46	134.7(6)
C48A−Zr1−C49A	33.8(5)	Zr1−O4−C27	112.6(6)
C47−Zr1−C48B	26.8(7)	C27−O4−C46	112.7(8)
C47−Zr1−C48A	29.8(5)	C48B−C47−C57	128(2)
O3−Zr1−O4	83.8(3)	C48A−C47−C57	123.6(16)
O2−Zr1−O3	84.0(2)	C47−C48A−C49A	123.3(16)
O1−Zr1−O4	82.5(3)	C48A−C49A−C50	118.8(14)
O1−Zr1−O2	82.2(3)	C47−C48B−C49B	132(3)
Zr1−O1−C1	174.6(6)	C48B−C49B−C50	122(3)
Zr1−O2−C45	131.2(6)	C49B−C50−C51	126(2)
Zr1−O2−C13	114.8(5)	C49A−C50−C51	122.1(13)

Table 4. Selected Bond Distances (Å) and Angles (deg) for Complex 7

Zr1−O1	1.957(3)	O2−C45	1.454(6)
Zr1−O2	2.316(4)	O3−C20	1.372(6)
Zr1−O3	1.957(3)	O4−C27	1.417(7)
Zr1−O4	2.311(4)	O4−C46	1.458(6)
Zr1−C47	2.172(6)	C47−C48	1.318(8)
Zr1−C48	2.192(6)	C47−C55	1.478(9)
O1−C1	1.346(7)	C48−C49	1.477(8)
O2−C13	1.411(7)		
C47−Zr1−C48	35.2(2)	C13−O2−C45	111.4(4)
O3−Zr1−O4	86.8(1)	Zr1−O3−C20	155.6(3)
O2−Zr1−O3	83.9(1)	Zr1−O4−C46	131.4(3)
O1−Zr1−O4	81.4(1)	Zr1−O4−C27	117.3(3)
O1−Zr1−O2	83.8(1)	C27−O4−C46	111.2(4)
Zr1−O1−C1	172.0(3)	C48−C47−C55	130.6(6)
Zr1−O2−C45	131.6(3)	C47−C48−C49	131.9(6)
Zr1−O2−C13	116.9(3)		

8, and **9**, respectively. In Table 7, a comparison of the relevant conformational parameters is reported. A, B, C, and D refer to the aromatic rings related to O1, O2, O3, and O4, respectively. The structure of **3** is shown in Figure 1.

Table 5. Selected Bond Distances (Å) and Angles (deg) for Complex 8

Zr1−O1	2.001(4)	O2−C13	1.413(9)
Zr1−O2	2.319(4)	O2−C45	1.454(8)
Zr1−O3	1.981(4)	O3−C20	1.354(8)
Zr1−O4	2.321(4)	O4−C27	1.400(8)
Zr1−N1	2.105(7)	O4−C46	1.441(8)
Zr1−N1′	2.105(7)	N1−C47	1.431(8)
O1−C1	1.325(8)		
N1−Zr1−N1′	76.9(2)	O1−Zr1−O2	82.8(2)
O4−Zr1−N1′	86.6(2)	N1−Zr1′−N1′	76.9(3)
O4−Zr1−N1	120.6(2)	Zr1−O1−C1	178.1(4)
O3−Zr1−N1′	96.1(2)	Zr1−O2−C45	127.5(4)
O3−Zr1−N1	154.1(2)	Zr1−O2−C13	121.6(4)
O3−Zr1−O4	83.2(2)	C13−O2−C45	110.9(5)
O2−Zr1−N1′	116.8(2)	Zr1−O3−C20	172.0(4)
O2−Zr1−N1	83.9(2)	Zr1−O4−C46	127.3(4)
O2−Zr1−O4	150.6(1)	Zr1−O4−C27	119.0(4)
O2−Zr1−O3	77.1(2)	C27−O4−C46	113.7(5)
O1−Zr1−N1′	157.3(2)	Zr1−N1−Zr1′	102.3(3)
O1−Zr1−N1	95.0(2)	Zr1′−N1−C47	131.9(5)
O1−Zr1−O4	79.4(2)	Zr1−N1−C47	125.4(5)
O1−Zr1−O3	99.7(2)		

Table 6. Selected Bond Distances (Å) and Angles (deg) for Complex 9[a]

Zr1−O1	1.988(5)	O1−C1	1.345(10)
Zr1−O2	2.445(6)	O2−C13	1.417(9)
Zr1−O5	1.974(7)	O2−C45	1.457(10)
Zr2−O3	1.985(6)	O3−C20	1.337(10)
Zr2−O4	2.492(4)	O4−C27	1.402(9)
Zr2−O5	1.987(7)	O4−C46	1.453(9)
O5−Zr1−O5′	76.4(3)	O3−Zr2−O4	78.7(2)
O2−Zr1−O5′	72.5(2)	Zr1−O1−C1	169.5(5)
O2−Zr1−O5	141.0(2)	Zr1−O2−C45	127.1(4)
O1−Zr1−O5′	128.0(2)	Zr1−O2−C13	122.1(5)
O1−Zr1−O5	105.8(2)	C13−O2−C45	110.8(6)
O1−Zr1−O2	76.8(2)	Zr2−O3−C20	171.4(5)
O5−Zr2−O5′	75.8(3)	Zr2−O4−C46	130.6(4)
O4−Zr2−O5′	144.7(2)	Zr2−O4−C27	116.9(4)
O4−Zr2−O5	71.2(2)	C27−O4−C46	112.5(6)
O3−Zr2−O5′	109.6(2)	Zr1−O5−Zr2	103.9(2)
O3−Zr2−O5	121.8(2)		

[a] Prime denotes a transformation of $-x, y, 0.5 - z$.

The overall geometry of the [*p*-Bu^t-calix[4]-(OMe)$_2$Zr] moiety, although similar to that observed in six-coordinate metal complexes,[6] is significantly different from that found in **2**. The four Zr−O bond distances are significantly longer in **3** than in **2**: 1.989(6) *vs* 1.914(3) Å and 2.355(6) *vs* 2.246(3) Å (average values for Zr−O1, Zr−O3 and Zr−O2, Zr−O4 couples, respectively). The O_4 core shows remarkable tetrahedral distortions ranging from −0.269(7) to 0.269(7) Å. Zirconium is displaced by 0.811(1) Å from the O_4 core toward butadiene.

The *s-cis*-butadiene is statistically distributed over two positions (A and B) tilted with respect to each other by 17.4(17)° and related by a *pseudo* mirror plane running through zirconium and bisecting the A and C aromatic rings. The Zr−C distances, which fall within a rather narrow range (2.398(17)−2.525(16) and 2.38(3)−2.51(3) for A and B, respectively) and the close C−C bond lengths within butadiene, averaging 1.43(2) and 1.44(4) Å for A and B, respectively, support the π^2,η^4 bonding mode. The planarity of the ligand as well as the *s-cis* conformation could be indicated by the C48−C49 internal torsion angle (0(2)° and 9(4)° for A and B, respectively). The plane of the ligand is nearly parallel

Table 7. Comparison of Relevant Conformational Parameters within Calixarene for Complexes 3, 4, 7, 8, and 9

	3	4	7	8	9
(a) Dihedral Angles (deg) between Planar Moieties[a]					
E^A	135.0(2)	147.3(2)	143.6(1)	139.7(2)	134.5(2)
E^B	98.7(2)	101.1(2)	108.7(1)	113.2(2)	110.3(2)
E^C	135.6(2)	136.8(2)	131.1(2)	147.4(2)	139.6(2)
E^D	99.1(2)	94.9(3)	108.4(1)	106.6(2)	95.5(2)
A^C	90.6(2)	104.0(3)	94.7(2)	107.1(2)	
B^D	162.2(3)	165.0(3)	142.7(2)	140.2(2)	
A^A′					90.9(2)
B^B′					139.3(3)
C^C′					99.2(2)
D^D′					168.9(3)
(b) Contact Distances (Å) between *para* Carbon Atoms of Opposite Aromatic Rings					
C4···C17	9.378(13)	9.793(12)	9.486(9)	9.733(10)	
C10···C24	6.043(12)	5.871(15)	6.989(8)	7.144(9)	
C4···C4′					9.189(13)
C10···C10′					7.317(13)
C17···C17′					9.661(14)
C24···C24′					5.688(11)

[a] E (reference plane) refers to the least-squares mean plane defined by the C7, C14, C21, C28 bridging methylenic carbons. A prime denotes a transformation of $-x, y, 0.5 - z$.

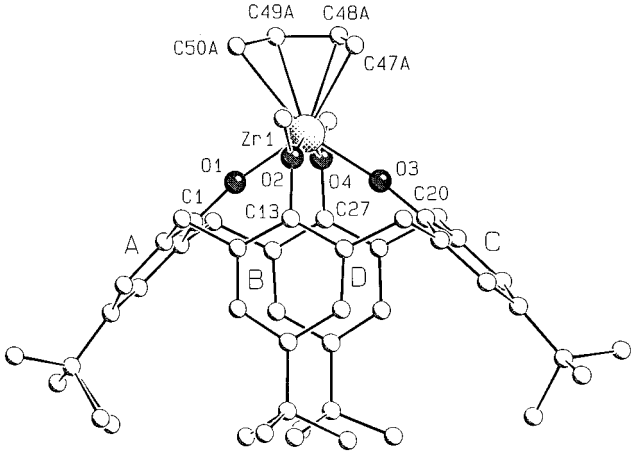

Figure 1. SCHAKAL view of complex **3**. Disorder has been omitted for clarity.

to the O_4 mean plane, the dihedral angle they form being 9.7(8)° and 7.7(14)° for A and B, respectively.

The elliptical cone section (Table 7) is different from that of **2**, the A and C opposite rings being nearly perpendicular (dihedral angle 90.6(2)° *vs* 108.2.(2)° in **2**) and the opposite B and C rings nearly parallel each other (dihedral angle 162.2(3)° *vs* 137.5(2)° in **2**). The contraction of the cavity is revealed by the narrow separation between the opposite C10···C24 *para* carbon atoms being shortened (6.043(12) Å *vs* 7.309(8) Å in **2**).

Crystals of **4** (Figure 2) contain benzene as a solvent of crystallization in a 1/1.5 Zr/C_6H_6 ratio. The four oxygen atoms of the O_4 core show remarkable tetrahedral distortion ranging from −0.308(6) to 0.303(6) Å, the zirconium atom projecting above the O_4 mean plane by 0.798(1) Å toward the butadiene unit. The trend of the Zr−O distances is similar to **3**. The butadiene fragment was found to be disordered over two positions (A and B) sharing the C47, C50 terminal carbon atoms, so only the C48 and C49 atoms appeared to be affected by disorder. The Zr−C distances, ranging from 2.427(10) to 2.505(12) Å and the localization of the terminal double bonds, support the π^2,η^4 bonding mode of butadiene. The torsion angles around the C48−C49 bond are 2(2)° and −12(5)° for A and B, respectively. The plane of the butadiene carbon atoms is nearly parallel to the O_4 mean plane, the dihedral angle being 9.1(7)° and 12.3(11)° for position A and B, respectively. The C51−C56 and C57−C62 phenyl rings are tilted with respect to the butadiene plane downward by 15.3(7)°, 20.7(9)° and 14.1(9)°, 6.6(7)° for A and B, respectively. The C51−C56 ring is oriented in such a way as to eclipse the A aromatic ring, the dihedral angle between them being 17.6(3)°. The C···C separations between opposite atoms range from 3.508(16) to 4.356(19) Å. The C57···C62 ring is twisted with respect the C aromatic ring by 43.3(6)°.

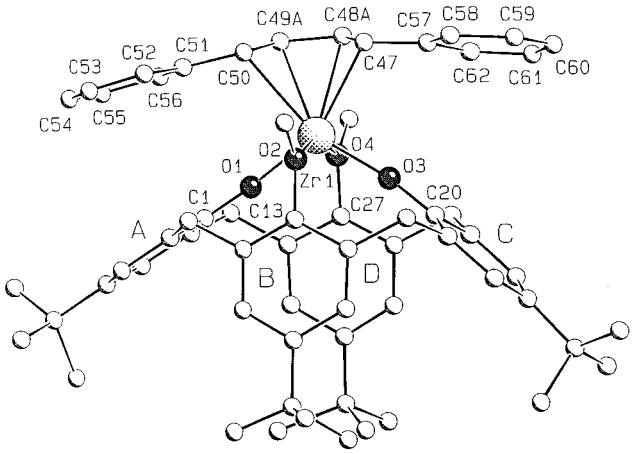

Figure 2. SCHAKAL view of complex **4**. Disorder has been omitted for clarity.

The calixarene ligand assumes an elliptical cone section with a conformation (Table 7) similar to that observed in complex **3** with the opposite A and C rings almost perpendicular (dihedral angle 104.0(3)°) and the B and D rings parallel (dihedral angle 164.0(3)°). Accordingly, the dimension of the cavity, indicated by the separations between opposite *p*-carbon atoms (C4···C17, 9.793(12) Å; C10···C24, 5.871(15) Å), is such to prevent the inclusion of guest molecules.

Although the bonding mode of the butadiene fragment in **3** and **4** is π^2,η^4, we should expect two general reactivity trends from the Zr−butadiene functionality. One forces the displacement of butadiene, thus making available the [*p*-Bu^t-calix[4]-$(OMe)_2(O)_2Zr^{II}$] fragment, the other leads to the insertion products, which would be expected for the σ^2,π,η^4 bonding mode.

Extended Hückel calculations[26,27] were performed to elucidate the nature of the bonding between the butadiene unit and the central metal in complex **3**. The ligand hereafter named *p*-Bu^t-calix[4]-$(OMe)_2(O)_2$ has been simplified by two phenoxo anions and two anisole molecules organized like in **3** according to a C_{2v} geometry. This simplified model retains the main features of the whole ligand; in particular, the geometrical constraints on the O_4 set of donor atoms has been maintained by fixing the geometry of the four phenoxo groups to the experimental values.

The coordination geometry of the butadiene unit was optimized with respect to the three parameters *R*, *L*, and θ depicted in Scheme 3, while all the other geometrical parameters were kept fixed to the experimental

(26) Hoffmann, R., Lipscomb, W. N. *J. Chem. Phys.* **1962**, *36*, 2179.
(27) Hoffmann, R. *J. Chem. Phys.* **1963**, *39*, 1397.

Scheme 3

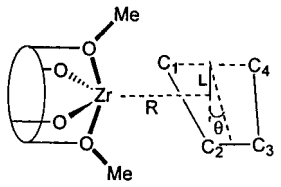

values. *R* describes the distance of the butadiene from zirconium, *L* defines its slide from the main symmetry axis (*z*) of the metal fragment, while θ denotes the dihedral angle between the butadiene plane and the fragment reference plane. The geometrical parameters taken for the metal fragment were Zr−O = 1.99 (phenoxy), Zr−O = 2.35 (Me−phenoxy), O−C(Ph) = 1.33 (phenoxy), O−C(Ph) = 1.41 (Me−phenoxy), O−C(Me) = 1.43, O−Zr−O = 114° (phenoxy), O−Zr−O = 153° (Me−phenoxy), Zr−O−C(Ph) = 172° (phenoxy), Zr−O−C(Ph) = 116° (Me−phenoxy), and Zr−O−C(Me) = 131°. The butadiene moiety was taken as a planar unit with C_1-C_2 = 1.43 Å, C_2-C_3 = 1.44 Å, C−H = 1.09 Å, $C_1-C_2-C_3$ = 120°, C−C−H = 120°.

The minimum was calculated for *R* = 1.9 Å, *L* = 0.6 Å, and θ = 12°, which corresponds to a π^2,η^4 structure and are in qualitative agreement with the experimental X-ray geometry. The electronic structure is analyzed in terms of the interactions between the frontier orbitals of the metal fragment and of the butadiene unit. The orbitals of the [*p*-Bu^t-calix[4]-$(OMe)_2(O)_2$Zr] fragment have already been discussed in detail,[6] and the resulting MO diagram is reported in the first column of Figure 3. We will recall only the main characteristics of this MO pattern here, which is characterized by four low-lying empty metal-based orbitals. The $d_{x^2-y^2}$ orbital, pointing more closely towards the oxygen ligands, is pushed high in energy, while the remaining four δ orbitals are found within 1 eV. Due to the reduced interaction with the methoxylated phenoxo ligands, the $1b_1(d_{xz})$ orbital is almost 1 eV lower in energy than $1b_2(d_{yz})$, with the $1a_1(d_{z^2})$ orbital only slightly higher. For a Zr^{II} fragment with a d^2 electron count, the lowest $1b_1$ orbital is doubly occupied and constitutes the HOMO.

On the extreme right of Figure 3, we show the frontier orbitals of butadiene, *i.e.*, the four π and π^* orbitals. The interaction between the [*p*-Bu^t-calix[4]-$(OMe)_2(O)_2$-Zr] fragment and the butadiene moiety is illustrated by the molecular orbital diagram for **3** in the central column of Figure 3.

The two most significant interactions can be seen in Figure 3. The empty $1b_2(d_{yz})$ orbital interacts with the occupied π_2 orbital, while the occupied $1b_1(d_{xz})$ orbital matches with the empty π_3^* and becomes the HOMO of the complex. The former interaction is of the donation type, while the latter describes the back-donation from the metal to butadiene. These interactions are similar to those observed in the [$Fe(CO)_3$(butadiene)] complex[28] and lead to an analogous π^2,η^4 bonding mode with all four carbon atoms of butadiene almost equally involved in the Zr−butadiene bond. This is confirmed by the overlap populations calculated for the optimized geometry of **3** and compared in Table 8 with literature values for the [$Fe(CO)_3$(butadiene)] and [Cp_2Zr-(butadiene)] complexes.[28] We see that in **3** all four Zr−C bonds show the same bond strength and also that the C_1-C_2 and C_2-C_3 bonds are equally strong.

The π^2 coordination mode of butadiene in **3** is very different from the $\sigma^2-\pi$ metallacyclopentene structure observed in [Cp_2Zr(butadiene)] (Scheme 4) and in other butadiene complexes of early transition metals.[1,29] This seemingly surprising difference is easily explained on the basis of the different frontier orbitals of the [*p*-Bu^t-calix[4]-$(OMe)_2(O)_2$Zr] and [Cp_2Zr] metal fragments. In the [Cp_2Zr] fragment, there is only one d_π orbital ($1b_2(d_{yz})$, interacting with π_2), while back-donation is described by the $1a_1-\pi_3^*$ mixing, which involves (as shown in Scheme 5) only the terminal carbons. Instead, in [*p*-Bu^t-calix[4]-$(OMe)_2(O)_2$Zr], a second d_π orbital ($1b_1(d_{xz})$) is available for the back-donation to π_3^*, all four carbon atoms being involved in such an interaction.

Figure 3 illustrates that a low-lying orbital of a_1 symmetry, almost degenerate with $1b_1$, is also available for the [*p*-Bu^t-calix[4]-$(OMe)_2(O)_2$Zr] fragment so that a $1a_1-\pi_3^*$ interaction would be expected for **3** leading to a quite stable $\sigma^2-\pi$ structure. To study this point, we performed EH (extended Hückel) calculations on **3** in which the dihedral angle θ was progressively increased from 10° (the optimal value for the π^2 structure) to 30°, which is a typical value for a $\sigma^2-\pi$ geometry. A small energy increase is observed, and the $\sigma^2-\pi$ structure is calculated only to be ca. 6 kcal mol^{-1} higher than the optimal π^2 one. Moreover, an analysis of the molecular orbitals shows that, on increasing θ, the HOMO shifts continuously from a $b_1-\pi_3^*$ to an $a_1-\pi_3^*$ character, reaching a mainly $a_1-\pi_3^*$ nature in the final $\sigma^2-\pi$ geometry. In other words, the [*p*-Bu^t-calix[4]-$(OMe)_2(O)_2$Zr] fragment has two low-lying almost degenerate b_1 and a_1 orbitals available for back-donation to the π_3^* orbital of butadiene, leading, respectively, to a π^2 and a $\sigma^2-\pi$ structure. The observed preference for the former structure is probably determined by the better $b_1-\pi_3^*$ overlap, but the $\sigma^2-\pi$ structure is easily available and may play an important role in the peculiar reactivity pattern of this butadiene complex.

It has to be mentioned that in the solid state structure of **3** the orientation of the butadiene unit is such that the plane bisecting the butadiene lies in the *xz* plane containing the two methoxy groups of the calix[4]arene ligand. This orientation is determined by the more favorable interaction of the butadiene π_2 and π_3^* orbitals with the two d_π orbitals of the the [*p*-Bu^t-calix[4]-$(OMe)_2(O)_2$Zr] fragment and also leads to a lower steric repulsion between the butadiene and the methoxy groups of the calix[4]arene ligand. An energy barrier for the rotation of the butadiene unit around the C_{2v} pseudo axis, leading to a rearrangement between the two possible configurations of the butadiene (Scheme 6), is then expected. To estimate this barrier, the alternative orientation with the plane bisecting the butadiene in the orthogonal *yz* plane has been calculated, reoptimizing *R*, *L*, and θ. An energy barrier of ~20 kcal mol^{-1} has been found, which is compatible with the observed ^{1}H NMR behavior.

Finally, we have also considered the *s-trans* butadiene complex in an attempt to understand why such an isomer is never observed in these zirconium−calixarene

(28) Tatsumi, K.; Yasuda, H.; Nakamura, A. *Isr. J. Chem.* **1983**, *23*, 145.

(29) Yasuda, H.; Tatsumi, K.; Okamoto, T.; Mashima, K.; Lee, K.; Nakamura, A.; Kai, Y.; Kanehisa, N.; Kasai, N. *J. Am. Chem. Soc.* **1985**, *107*, 2410.

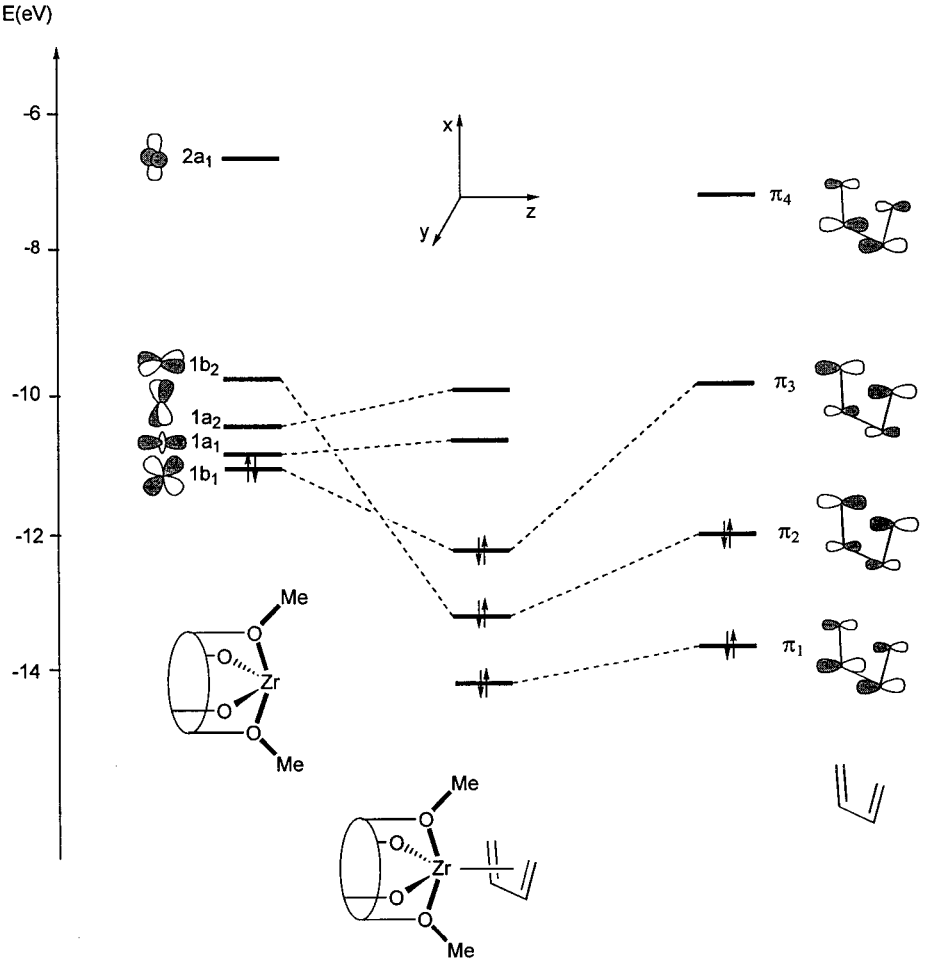

Figure 3. Orbital interaction diagram for Zr(calix[4]arene) and butadiene.

Table 8. Comparison of the Calculated Overlap Populations in 3 with Those for [Cp_2Zr(butadiene)][28] and [$Fe(CO)_3$(butadiene)][28]

	3	[$Fe(CO)_3$(butadiene)]	[Cp_2Zr(butadiene)]
$M-C_1$	0.237	0.202	0.338
$M-C_2$	0.218	0.184	0.060
C_1-C_2	0.961	0.979	0.991
C_2-C_3	0.971	0.974	1.012

Scheme 4

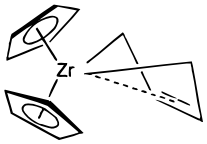

Scheme 5

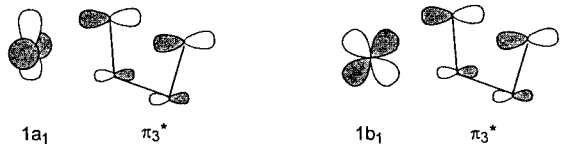

systems. Our analysis followed the procedures of ref 28, according to which the stability of the [Cp_2Zr(diene)] *s-trans* complexes is attributed to the comparable overlap of the *s-trans*-π_3* and *s-cis*-π_3* orbitals with the $1a_1$ orbital of the metal fragment. On the other hand, for most of the familiar metal−diene complexes like [Fe-($CO)_3$(butadiene)], the metal fragment only has a donor orbital of d_π symmetry and its overlap with *s-trans*-π_3* is much smaller than that with *s-cis*-π_3*. This explains why *s-trans*-butadiene complexes are so rare. In the [*p*-Bu^t-calix[4]-($OMe)_2(O)_2$Zr] fragment, the $b_1(d_{xz})$ orbital overlaps much better with *s-cis*-π_3* than with the *s-trans*-π_3*, suggesting an instable *s-trans* isomer. However, a low-energy a_1 orbital is also available so that the *s-trans* isomer is not expected to be too high in energy. Accordingly, our calculations give the *s-trans* isomer to be *ca.* 15 kcal mol^{-1} higher in energy than the *s-cis* isomer. This energy difference, although seemingly small, is high enough to prevent the detection of any *s-trans* isomer in equilibrium conditions. Note that for the [Cp_2Zr(butadiene)], which shows an equilibrium between the *s-cis* and *s-trans* isomers, an energy barrier of *ca.* 2 kcal mol^{-1} has been calculated at extended Hückel level.[28]

Scheme 6

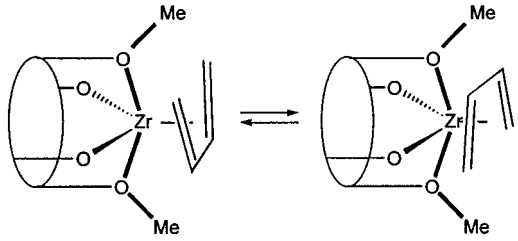

In connection with the *s-trans* form, a π,η^2 butadiene coordination mode has often been proposed as an intermediate in zirconocene−butadiene chemistry.[1b] As we never observed the *s-trans* isomer and all the products obtained in insertion reactions can be rational-

Scheme 7

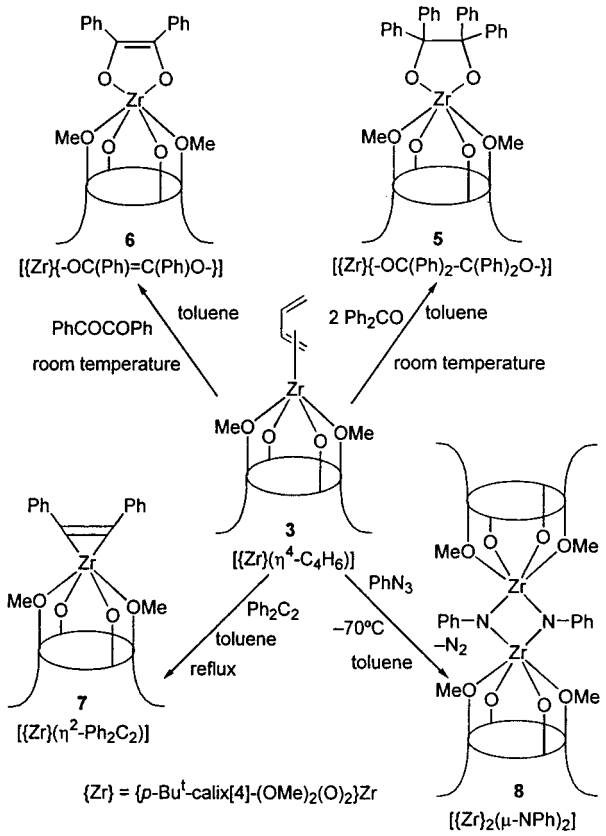

ized by the σ^2,π,η^4 model, the intermediacy of such a high-energy η^2 butadiene complex does not seem to play any role here. Therefore, the latter form will not be discussed in detail.

Displacement Reactions. Scheme 7 displays reactions where **3** behaves as a source of a Zr(II) derivative. They can be formally viewed as oxidative additions to the [*p*-Bu^t-calix[4]-(OMe)$_2$(O)$_2$Zr] fragment.

The main driving force in the case of ketones is the high oxophilicity of the metal, which induces the reductive coupling of benzophenone leading to **5** or the addition of dibenzoyl causing the formation of the dioxometallacycle in **6**, which contains a C−C double bond. It has to be mentioned that the reaction of **3** with ketones at low temperature (*vide infra*) follows a very different pathway and leads to the insertion of the carbonylic group into a Zr−C σ bond. In the reaction with **3**, phenylazide functions as a source of phenylnitrene,[30] leading to the corresponding Zr(IV)-dimeric phenylamido derivative.

Displacement of butadiene with diphenylacetylene[1a] occurs under more drastic conditions. We should comment on the nature of the complexes **5**−**8**. All of these complexes have been analytically and spectroscopically characterized and the ^{1}H NMR can be, in this sense, particularly informative. Complexes **5** and **6** show two pairs of doublets and a single methoxy group along with two singlets for the Bu^t groups. This apparent C_{2v} symmetry is not only seen at room temperature, but is maintained also at low temperature (243 K). Complexes **5** and **6** form equally well from the corresponding [{*p*-Bu^t-calix[4]-(OMe)$_2$(O)$_2$}Zr(R$_2$C-X)] (X = O, NR) zirconium−imine/ketone derivatives.[6b] The formation of the η^2-monoacetylene complex, **7**, is a rare event in the general context of zirconium organometallic chemistry, namely with alkoxo and cyclopentadienyl ancillary ligands, which are the most widely used. A complex like **7** has been proposed as an intermediate in the formation of zirconopentadiene, coming from the reductive coupling of the diphenylacetylenes and isolated as the PMe$_3$ adduct.[31] Due to its unusual occurrence, **7** has been structurally characterized by an X-ray analysis, while the ^{1}H NMR spectrum shows a typical C_{2v} symmetry for the calix[4]−Zr fragment.

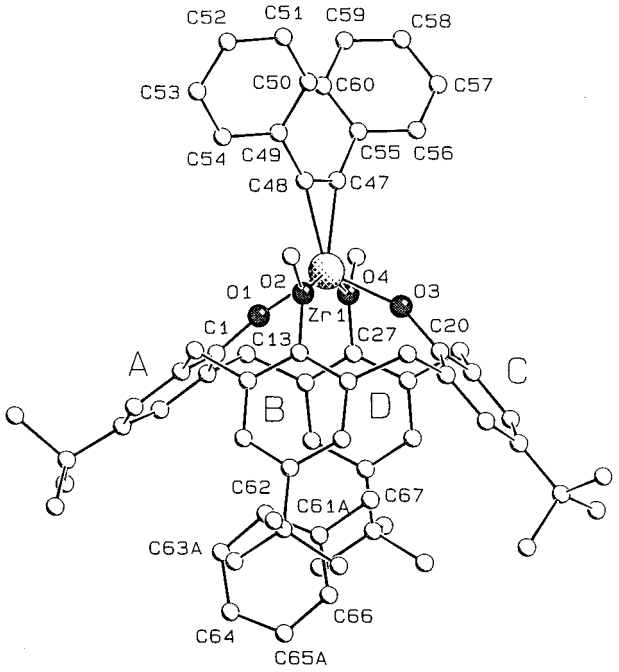

Figure 4. SCHAKAL view of complex **7**. Disorder has been omitted for clarity.

Crystals of **7** (Figure 4) contain toluene as a solvent of crystallization in a 1/4.5 Zr/C$_7$H$_8$ ratio. The O$_4$ core is tetrahedrically distorted, displacements ranging from −0.206(3) to 0.213(3) Å. Zirconium protrudes from it toward the alkene ligand by 0.720(1) Å, while the Zr−O bond trend is similar to **3** and **4**. The diphenylacetylene displays a nearly symmetric bonding mode to the metal, with very close bond distances (Zr−C47, 2.172(6) Å; Zr−C48, 2.192(6) Å). The C47−C48 bond distance (1.318(8) Å) is consistent with a double-bond character. The plane through the η^2-bonded atoms (Zr, C47, C48) is perpendicular to the O$_4$ mean plane (dihedral angle 89.8(2)°) and forms dihedral angles of 42.9(3)° and 46.0(3)° with the C49−C54 and C55−C60 phenyl rings, respectively. The calixarene macrocycle assumes an elliptical cross-section conformation (Table 7). The B and D rings form a dihedral angle of 142.7(2)° *vs* 162.2-

(30) Cenini, S.; La Monica, G. *Inorg. Chim. Acta* **1976**, *18*, 279. Osborne, J. H.; Rheingold, A. L.; Trogler, W. C. *J. Am. Chem. Soc.* **1985**, *107*, 7945. Gambarotta, S.; Chiesi-Villa, A.; Guastini, C. *J. Organomet. Chem.* **1984**, *270*, C49. Nugent, W. A.; Haymore, B. L. *Coord. Chem. Rev.* **1980**, *31*, 123. Hubert-Pfalzgraf, L. G.; Aharonian, G. *Inorg. Chim. Acta* **1985**, *100*, L21.

(31) Negishi, E.-I.; Takahashi, T. *Acc. Chem. Res.* **1994**, *27*, 124. van Wagenen, B. C.; Linghouse, T. *Tetrahedron Lett.* **1989**, *30*, 3495. Takahashi, T.; Swanson, D. R.; Negishi, E.-I. *Chem. Lett.* **1987**, 623. Buchwald, S. L.; Watson, B. T. *J. Am. Chem. Soc.* **1987**, *109*, 2544. Lefeber, C.; Baumann, W.; Tillack, A.; Kempe, R.; Görls, H.; Rosenthal, U. *Organometallics* **1996**, *15*, 3486. Rosenthal, U.; Ohff, A.; Baumann, W.; Tillack, A. *Z. Anorg. Allg. Chem.* **1995**, *621*, 77. Rosenthal, U.; Ohff, A.; Michalik, M.; Görls, H.; Burlakov, V. V.; Shur, V. B. *Angew. Chem., Int. Ed. Engl.* **1993**, *32*, 1193.

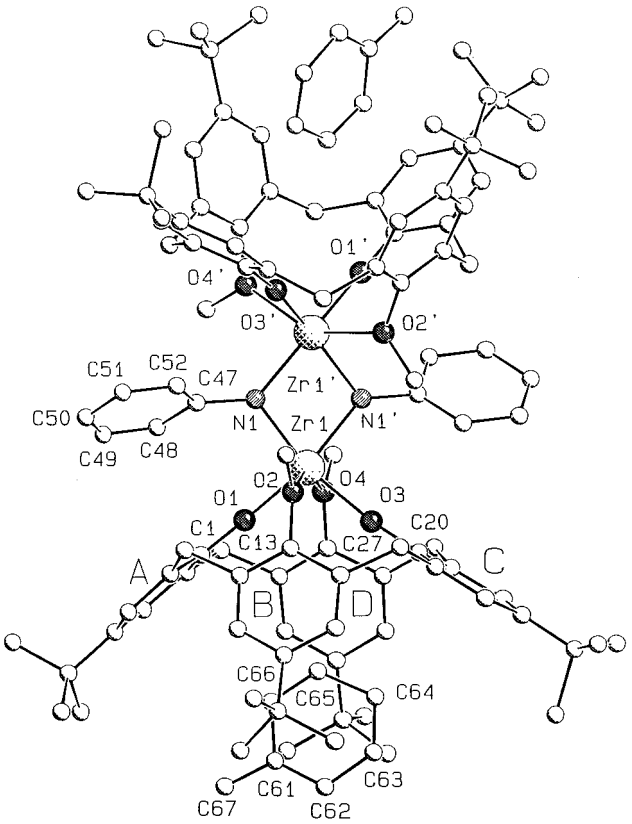

Figure 5. SCHAKAL view of complex **8**. Disorder has been omitted for clarity. Prime denotes a transformation of $-x$, y, $0.5 - z$.

(3)° and 164.0(3)° in **3** and **4**, respectively. Consequently, a remarkable lengthening of the distance between the opposite *p*-carbon atoms is observed (C10···C24, 6.989(8)°). This separation, which is comparable to that observed in **2**, allows the inclusion of a toluene molecule.

A particularly interesting synthetic approach to the imido derivative **8** concerns the reaction of **3** with phenylazide. The synthesis of zirconium imido compounds in the bis(cyclopentadienyl) series has been mainly achieved by amine or alkane elimination from the corresponding diamido or dialkylamido derivatives.[32] The imido derivative occurs in the dimeric form like **8**, eventually in equilibrium with the corresponding monomeric one to which it is associated.[32a] There is no evidence in the present case of any relationship between **8** and the corresponding monomeric form, though the steric conditions would be favorable to it. Further, this is the first example of a zirconium−imido functionality associated with alkoxo ancillary ligands. The structure of **8** is given in Figure 5.

Crystals of **8** contain toluene as a solvent of crystallization in a 1/4 Zr/C_7H_8 ratio. Coordination around zirconium is distorted octahedral, the best equatorial plane being defined by the O2, O3, O4, N1 atoms, the O1 and N1′ atoms assuming a *trans* arrangement (O1−Zr−N1′, 157.3(2)°; prime denotes a transformation of $-x$, y, $0.5 - z$). As is usually observed for six-coordinate calixarene metal complexes, the O_4 core shows remarkable tetrahedral distortion (displacement ranging from −0.352(4) to 0.357(4) Å); zirconium being displaced by 0.935(1) Å toward the imido atoms. The Zr_2N_2 mean plane is nearly perpendicular to the O_4 core (dihedral angle 81.9(2)°). Phenylimido bridges two Zr atoms at a distance of 3.279(1) Å. The complex has a crystallographically imposed C_2 symmetry with the 2-fold axis perpendicular to the mean plane through the Zr_2N_2 core center of gravity. The Zr−N bond distance (2.105(7) Å) is a little longer than those found for $[\{(\mu\text{-NPh})ZrCl_2(thf)_2\}_2]$[33] and $[\{(\mu\text{-NBu}^t)Zr(NMe_2)_2\}_2]$.[32b]

Insertion Reactions. Although the bonding mode of butadiene to zirconium is π^2,η^4, as revealed by the X-ray analysis, in a number of reactions and under certain conditions it behaves like a σ^2,π,η^4 butadiene, thus the zirconium−butadiene functionality behaves as though it contains two Zr−C σ bonds. This behavior is illustrated in the reactions listed in Scheme 8.

These reactions include the hydrolysis to form the μ-dioxo dimer **9** and the products derived from the formal insertion of nitriles, ketones, and Bu^tNC into the Zr−C σ bonds. In the case of hydrolysis, butenes have been identified. The occurrence of the zirconyl compound in a monomeric form remains rather rare.[34] The ^1H NMR spectrum of **9** is in agreement with an approximate D_2 symmetry and, thus, shows a singlet for the methoxy groups and a pair of doublets for the bonding methylene. The structural peculiarities have been disclosed by an X-ray analysis (Figure 6).

Crystals of **9** (Figure 6) contain toluene and *n*-hexane as solvents of crystallization in a 1/1/2 dimer/toluene/*n*-hexane ratio. The complex has a crystallographically imposed C_2 symmetry, the 2-fold axis running through the two zirconium atoms. The O_4 cores are tetrahedrically distorted (displacements ranging from −0.191(4) to 0.191(4) Å), Zr1 and Zr2 protruding by 0.931(1) and 0.933(1) Å from the corresponding O_4 mean planes toward the oxo bridges. The mean plane through the zirconium atoms and the O5 oxygen atoms is strictly perpendicular to the O_4 mean planes from symmetry requirements. The Zr1···Zr2 and O5···O5′ separation within the Zr_2O_2 system are 3.120(1) and 2.440(7) Å, respectively. Zirconium is in a very distorted six-coordination geometry. The Zr−O5 bond distances (mean value 1.981(7) Å) are close to those found in a series of complexes containing the $[Zr_2(\mu\text{-O})_2]$ moiety (mean value 1.953(3) Å averaged over 29 entries). The Zr1−O1 and Zr2−O3 bond distances are close to those in **4** and **7**, while the Zr1−O2 and Zr2−O4 bond distances (mean value 2.469(6) Å) are significantly longer as a consequence of some intraligand interactions. The elliptical cone section conformation assumed by the two calixarene ligands (Table 7) is significantly different. The macrocycle related to the Zr1 atom shows a conformation almost similar to that observed in **7** and **8** (C10···C10′, 7.317(13) Å; prime denotes a transformation of $-x$, y, $0.5 - z$) and the dimension of the cavity allows a toluene molecule to be included as a guest. The geometry of a macrocycle related to Zr2 compares better with that observed in **3** and **4**, from the C24···C24′ (5.688(11) Å) separation.

(32) (a) Walsh, P. J.; Hollander, F. J.; Bergman, R. G. *J. Am. Chem. Soc.* **1992**, *110*, 8729. (b) Nugent, W. A.; Harlow, R. L. *Inorg. Chem.* **1979**, *18*, 2030 and references therein.

(33) Polamo, M.; Mutikainen, I.; Leskelä, M. *Acta Crystallogr. Sect. C: Cryst. Struct. Commun.* **1996**, *52*, 1082.

(34) Lee, S. Y.; Bergman, R. G. *J. Am. Chem. Soc.* **1996**, *118*, 6396. Jacoby, D.; Floriani, C.; Chiesi-Villa, A.; Rizzoli, C. *J. Am. Chem. Soc.* **1993**, *115*, 7025. Howard, W. A.; Waters, M.; Parkin, G. *J. Am. Chem. Soc.* **1993**, *115*, 4917. Carney, M. J.; Walsh, P. J.; Hollander, F. J.; Bergman, R. G. *Organometallics* **1992**, *11*, 761.

Scheme 8

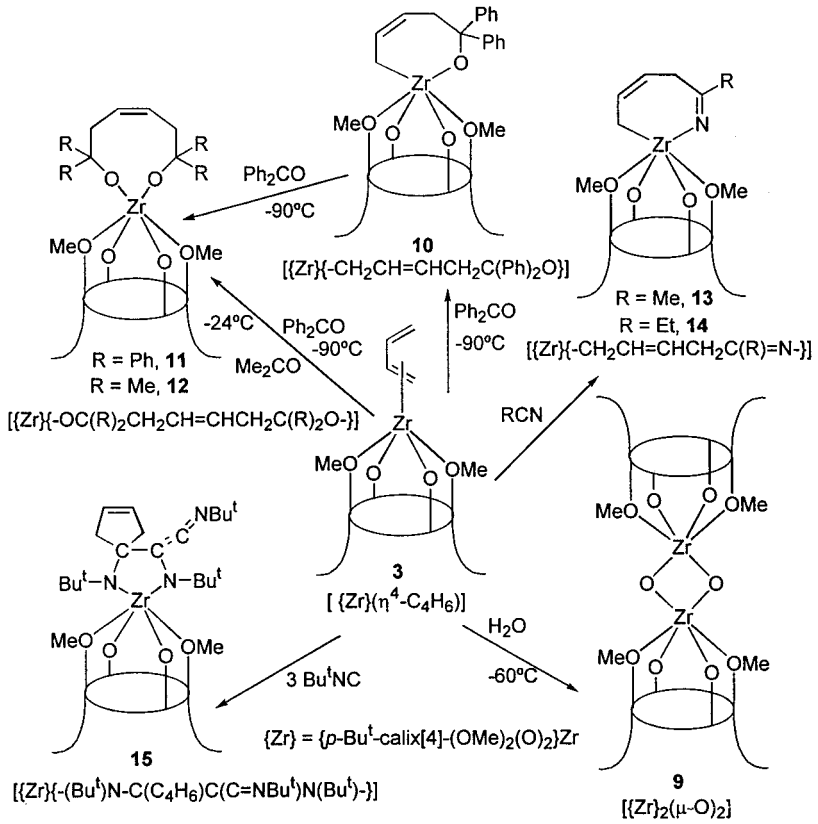

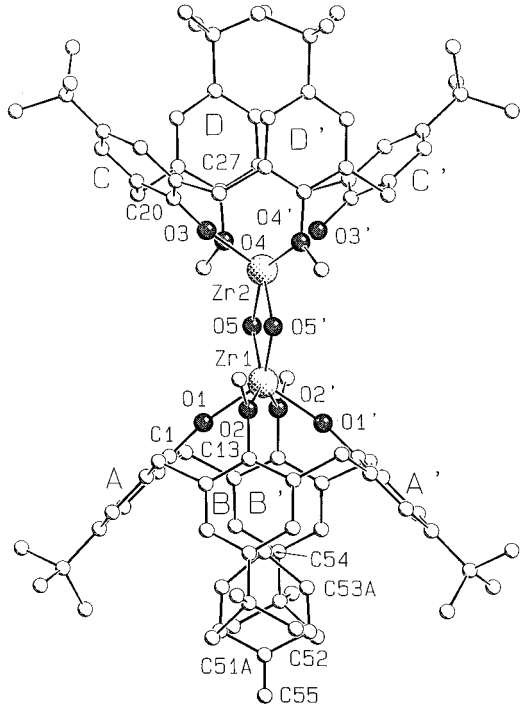

Figure 6. SCHAKAL view of complex **9**. Disorder has been omitted for clarity. Prime denotes a transformation of $-x$, y, $0.5 - z$.

The reaction of **3** with ketones has a particular dependence on the temperature. When it was performed at room temperature (see Scheme 7, compounds **5** and **6**), we observed the displacement of butadiene by the incoming substrate. On the contrary, when the reaction was carried out at low temperature and with a 1:1 molar ratio (Scheme 8), the insertion of the ketone unit was observed in one of the two Zr−C σ bonds, leading to the seven-membered metallacyle in **10**. The reaction then proceeds further with a second mole of Ph_2CO to give **11**.[1b] The proposed structures for **10** and **11** have been supported by the elemental and spectroscopic analyses. Above 40 °C, compound **10** exhibits a ^{1}H NMR spectrum of C_{2v} symmetry: one pair of doublets for the bridging methylene groups and a singlet for the methoxy groups. It should be noted that the pattern of the protons of the organic fragment bound to the metal remains unchanged in the range of temperatures from 25 to 70 °C. A dynamic process increases the apparent symmetry of the compound in solution, but a clear low-symmetry spectrum cannot be seen even at the low-temperature limit. On the other hand, at low temperature, compound **11** shows a spectrum of C_s symmetry, with two pair of doublets for the bridging methylene groups, three singlets for the Bu^t groups, and two singlets for the methoxy groups; three multiplets for the organic fragment protons bound to the metal are visible, as is the case for the diene complex **3**. Above 60 °C, compound **11** exhibits a ^{1}H NMR spectrum with C_{2v} symmetry: one pair of doublets for the bridging methylene groups and a singlet for the methoxy groups; two of the three multiplets corresponding to the butadiene fragment collapse to give a single broad signal. A structural model for the nine-membered dioxo metallacycle **11** has been supported by preliminary X-ray results on **12**, derived from the insertion of two molecules of acetone on **3**, behaving as a dialkyl−zirconium derivative. The structural data confirm, in particular, the *cis* stereochemistry of the C=C bond, at variance with what is often found in zirconocene chemistry.[23]

Unlike in the case of [Cp_2Zr(butadiene)] complexes,[35] complex **3** inserts a single molecule of nitrile, leading to complexes **13** and **14**. For both compounds, the ^{1}H

NMR spectrum shows C_1 symmetry at room temperature with the appearance of four pairs of doublets for the bridging methylenes, two singlets for the methoxy groups, and four singlets for the Bu^t substituents. A preliminary X-ray analysis on **14** (see Supporting Information) confirms the proposed structure, which serves also as a structural model for **10**.

The reaction of **3** with Bu^{t}NC emphasizes its behavior as a σ^2,π,η^4 metal-bonded butadiene. The reaction proceeds as in the case of the dialkyl derivatives [{*p*-Bu^t-calix[4]-(OMe)$_2$(O)$_2$}Zr(R)$_2$] and consumes 3 equiv of the isocyanide.[6b] The pathway leading to **15** has been clarified in the latter case, and it goes through the preliminary formation of a η^2-imine which further inserts a molecule of isocyanide to give a carbenoid structure, which couples with the third equivalent of Bu^{t}NC.[36] Unlike the dialkyl derivative, we were not able to isolate the intermediate η^2-imino complex. Complex **15** has C_1 symmetry, and its ^{1}H NMR spectrum shows four pairs of doublets for the bridging methylene groups, two singlets for the MeO groups, and three singlets for the Bu^t groups. This spectrum resembles the analogous complex derived from the reaction of [{*p*-Bu^t-calix[4]-(OMe)$_2$(O)$_2$}Zr(Me)$_2$] with 3 equiv of Bu^{t}NC, whose structure has been determined by an X-ray analysis. The IR data are also very close for the two compounds (ν(C−N), cm^{-1}: 1968 *vs* 1964.6 for **15**).

Conclusions

This work emphasizes the two reaction paths accessible to *s-cis* π^2,η^4 butadiene bound to a formal Zr(II) supported by a tetraoxo dianionic matrix: (i) 1,1 insertion reactions into the terminal Zr−C bonds, best visualized in the σ^2,η^4 description of the complex; (ii) reactions where the butadiene ligand is displaced, making available the tetraoxo−zirconium(II) fragment to a variety of coordinative and oxidative addition reactions.

The main differences with the corresponding [Cp$_2$Zr]-based chemistry are: (i) the [*p*-Bu^t-calix[4]-(OMe)$_2$(O)$_2$-Zr] fragment promotes multiple insertions, as exemplified by the obtention of a spyro, cumulenic product **15** from the insertion of 3 equiv of isocyanide; (ii) the butadiene ligand can be displaced under very mild conditions, especially when reacted with polar ligands, leading to thermodynamically favored species, the best example being the formation of the phenylimido complex **8** from the reaction with phenylazide. The obtention of the remarkably stable diphenylacetylene complex **7** illustrates the exceptional ability of the [*p*-Bu^t-calix[4]-(OMe)$_2$(O)$_2$Zr] fragment to stabilize unsaturated fragments without the need of added ligands, explained by the peculiar facial arrangement of the three lowest-lying metal orbitals.

Acknowledgment. We thank the "Fonds National Suisse de la Recherche Scientifique" (Bern, Switzerland, Grant No. 20-46′590.96), Ciba Specialty Chemicals (Basle, Switzerland), and Fondation Herbette (University of Lausanne, N. Re) for financial support.

Supporting Information Available: X-ray crystallographic files, in CIF format, for complexes **3**, **4**, **7**−**9**, and **14** are available on the Internet only. Access information is given on any current masthead page.

OM970624M

(35) Erker, G.; Pfaff, R. *Organometallics* **1993**, *12*, 1921. Erker, G.; Pfaff, R.; Kowalski, D.; Würthwein, E.-U. *J. Org. Chem.* **1993**, *58*, 6771.

(36) The coupling of isocyanides with (transient) carbenoids to give cumulenes is well-estabilished, see: Moloy, K. G.; Fagan, P. J.; Manriquez, J. M.; Marks, T. J. *J. Am. Chem. Soc.* **1986**, *108*, 56. Valero, C.; Grehl, M.; Wingbermühle, D.; Kloppenburg, L.; Carpenetti, D.; Erker, G.; Petersen, J. L. *Organometallics* **1994**, *13*, 415. Scott, M. J.; Lippard, S. J. *J. Am. Chem. Soc.* **1997**, *119*, 3411.